Journal of Environmental Chemical Engineering 14 (2026) 121864

Contents lists available at ScienceDirect

Journal of Environmental Chemical Engineering

journal homepage: www.elsevier.com/locate/jece

Oxidative denitrogenation using sustainable carbon nanotubes: Effect of reaction conditions on hydrogen peroxide efficiency

Fernanda F. Roman [a,b,c,*], Adriano S. Silva [a,b,c], Jose L. Diaz de Tuesta [d], Adrián M.T. Silva [b,c], Joaquim L. Faria [b,c], Helder T. Gomes [a,**]

[a] CIMO, LA SusTEC, Instituto Politécnico de Bragança, Campus de Santa Apolónia, Bragança 5300-253, Portugal
[b] LSRE-LCM - Laboratory of Separation and Reaction Engineering – Laboratory of Catalysis and Materials, Faculty of Engineering, University of Porto, Rua Dr. Roberto Frias, Porto 4200-465, Portugal
[c] ALiCE - Associate Laboratory in Chemical Engineering, Faculty of Engineering, University of Porto, Rua Dr. Roberto Frias, Porto 4200-465, Portugal
[d] Chemical and Environmental Engineering Group, ESCET, Universidad Rey Juan Carlos, c/Tulipán s/n, Móstoles 28933, Spain

ARTICLE INFO

Dataset link: Dataset for paper "Oxidative denitrogenation using sustainable carbon nanotubes: Effect of reaction conditions on hydrogen peroxide efficiency"

Keywords:
Process optimization
Plastic solid waste valorization
Waste-derived catalyst
Fuel purification
Hydrogen peroxide consumption

ABSTRACT

Nitrogenated compounds in fuels contribute significantly to NO_x emissions, prompting the need for efficient and sustainable removal technologies. Oxidative denitrogenation (ODN) has emerged as an alternative or complement to hydrodenitrogenation (HDN) to remove undesired nitrogenated compounds. While ODN requires significantly milder conditions compared to HDN, it relies on the use of hydrogen peroxide as oxidant source. Most works report the removal of nitrogenated compounds but neglect the rate of consumption and efficiency of use of hydrogen peroxide. In this work, the operational conditions during ODN (hydrogen peroxide concentration, catalyst concentration, temperature, and pH) were optimized to maximize the removal of nitrogenated compound, using quinoline as model compound, from a simulated fuel. Two sustainability-oriented parameters were introduced: (i) the abatement of total organic carbon and (ii) the efficiency of hydrogen peroxide consumption. Under optimum conditions ($[H_2O_2]_0$ = 12 g L^{-1}, 70 °C, [cat] = 2.5 g L^{-1}, pH_0 = 3.0), the process achieved 89 % quinoline removal, 35 % TOC abatement, and more than 77 % H_2O_2 consumption efficiency. These results demonstrate the potential of ODN to operate under mild conditions while maintaining high oxidant efficiency for model nitrogen-containing fuel compound, contributing to cleaner and more sustainable fuel purification strategies.

1. Introduction

Nitrogen-containing compounds in fuel oils are a major environmental concern due to their contribution to NO_x emissions during engine combustion [1], which are linked to air pollution and acid rain [2]. Conventional hydrodenitrogenation (HDN) processes, although effective, are energy-intensive and costly ($T > 300$ °C, P_{H2} = 6–14 MPa) [3], prompting the need for alternative, more sustainable methods. Among them, oxidative denitrogenation (ODN) has emerged as a promising approach [1,4]. ODN reactions are typically carried out under atmospheric pressure and moderate temperatures (<150 °C) [1], using oxidants (most commonly hydrogen peroxide, and less commonly organic peroxides or ozone) in biphasic systems involving an extractant solvent [5]. During ODN, the nitrogen-containing molecules are oxidized into more polar compounds that can be easily removed by liquid extraction [1]. The milder operating conditions and reduced energy demands make ODN attractive for cleaner fuel purification strategies.

A major challenge in the development of viable ODN processes is the selection of efficient and environmentally responsible catalysts. Previous work has shown that reaction rate is highly influenced by the mass transfer of nitrogenated compounds from the fuel to the extractant phase, requiring catalysts that also act as phase-transfer promoters [5]. Carbon nanotubes (CNTs) are particularly suitable in this regard: they can catalyze the decomposition of hydrogen peroxide into hydroxyl radicals [6], drive the oxidation and mineralization of various organic molecules [7–9], and enhance phase transfer in biphasic oxidations [5,10,11]. Their performance is further improved by the ease with which their surface chemistry can be tuned [12,13]. Importantly, CNTs can be

* Corresponding author at: CIMO, LA SusTEC, Instituto Politécnico de Bragança, Campus de Santa Apolónia, Bragança 5300-253, Portugal.
** Corresponding author.
E-mail addresses: roman@ipb.pt (F.F. Roman), htgomes@ipb.pt (H.T. Gomes).

https://doi.org/10.1016/j.jece.2026.121864
Received 17 December 2025; Received in revised form 10 February 2026; Accepted 17 February 2026
Available online 18 February 2026

produced from plastic solid waste (PSW) [7,14,15], providing high surface area and favourable electronic properties while also enabling PSW valorization, addressing waste accumulation concerns [16] and supporting resource recovery [17].

Despite growing interest in ODN, most studies focus primarily on the removal of nitrogenated compounds and often employ large excesses of oxidant [18–26], without systematically evaluating oxidant efficiency or utilization. As a result, a critical knowledge gap remains regarding how reaction conditions, such as hydrogen peroxide concentration, temperature, catalyst loading, and pH, govern both denitrogenation performance and oxidant efficiency in biphasic ODN systems. Excessive use of hydrogen peroxide raises economic and environmental concerns [27], making its efficient consumption a critical parameter for sustainable operation. Likewise, total organic carbon (TOC) measurements in the aqueous phase offer important insights into the fate of both nitrogenous and non-nitrogenous species, yet TOC analysis is rarely reported in ODN studies. Addressing these gaps requires approaches that combine process optimization with sustainability-oriented performance indicators.

In this study, we provide a comprehensive evaluation of the oxidative denitrogenation process in a model biphasic fuel system using PSW-derived carbon nanotubes, systematically examining key operational parameters and introducing two complementary sustainability metrics: TOC abatement and hydrogen peroxide consumption efficiency. Hydrogen peroxide was selected as the oxidant due to its widespread use in ODN and its environmentally benign decomposition into water and oxygen [1]. Quinoline (QN) was selected as representative nitrogen-containing model compound due to its frequent use in ODN studies, enabling direct comparison with previously reported systems. Pyridine (PYR) was additionally evaluated due to its higher resistance to oxidation [28], to assess the robustness of the optimized ODN conditions toward more recalcitrant nitrogen-containing species. While the study is conducted using model compounds and simulated fuel, the results provide operational insights relevant to the rational design of more sustainable ODN processes.

2. Materials and methods

2.1. Reactants and materials

The materials and reactants used are described in Text S1.

2.2. Synthesis and characterization of materials

Carbon nanotubes were synthesized by chemical vapour deposition (CVD) of pyrolysis gases from polymer, which requires a metal catalyst for the CVD section. Both methodologies to synthesize CVD catalyst and CNTs are reported below.

2.2.1. Synthesis of CVD catalyst

The chemical vapor deposition (CVD) catalyst was obtained by sol-gel [29]. An ethanolic solution containing 0.5 M of Ni^{2+} was heated until reaching its boiling point, and a 0.25 M solution of Fe^{3+} in ethanediol was heated to 60 °C (5 min). Then, both solutions were submerged in ice until reaching temperature equilibrium, following procedures previously reported [30]. When the desired temperature was reached, the two solutions were mixed in one beaker containing Al_2O_3 (6.6 g). The mass of alumina was calculated to allow a deposition of 20 % of the active phase into the Al_2O_3 surface. The mixture was heated to 60 °C for 2 h, followed by increase of the temperature to 120 °C, until reaching a gel-like texture (*ca.* 3 h), which was followed by a temperature increase to 200 °C, until a powder was obtained (*ca.* 3 h). The powder recovered in the end was thermally treated under air atmosphere at 850 °C for 3 h, leading to NiFe.

2.2.2. Synthesis of carbon nanotubes

The CVD growth of the carbon nanostructures was carried out in a vertical oven (TH/TV, Termolab) and follows a similar procedure as previously reported [5,7]. Briefly, 1 g of the catalyst (NiFe) was loaded in the lower region and 5 g of the carbon source was loaded in the upper region. The carbon source chosen for this work was a mixture of polyolefins (POL) simulating a composition of plastics typically found in PSW (35 % of low-density polyethylene (LDPE), 25 % of high-density polyethylene (HDPE) and 40 % of polypropylene (PP)), as reported elsewhere [31]. The reaction was carried out at $T = 800$ °C with a 0.5 h hold time under nitrogen flow (50 cm^3 min^{-1}), leading to POL@NiFe. The mass yield was calculated according to Eq. (1).

$$Yield\ (\%) = \frac{m_{recovered} - m_{catalyst}}{m_{polyolefin} \times \%C_{polymer}} \quad (1)$$

in which $m_{recovered}$ is the mass of the sample recovered after the CVD process accounting for both organic and inorganic phases (in g), $m_{catalyst}$ is the mass of catalyst loaded in the reactor (in g), $m_{polyolefin}$ is the mass of the polymer (in g), and $\%C_{polymer}$ is the carbon content in the starting material (85.6 *wt.*% for LDPE, HDPE and PP [32]). After synthesis, POL@NiFe was subject to two distinct treatments: (i) H_2SO_4 washing and (ii) a HNO_3 oxidation, which generated 2 different materials. The washing with H_2SO_4 aimed at reducing the quantity of metallic particles attached to the CNT structure, and it was carried out at 140 °C for 3 h under reflux, with a 50 % v/v H_2SO_4 solution and a POL@NiFe nanoparticle concentration of 20 g L^{-1}. After cooling the solution to room temperature, the material was thoroughly washed until the rising waters reached neutrality, leading to POL-P@NiFe. The nitric acid oxidation aimed at introducing oxygenated groups on POL@NiFe surface. The reaction was carried out at 130 °C for 24 h under reflux, with a 15 M HNO_3 solution, and a POL@NiFe particle concentration of 50 g L^{-1}, as reported elsewhere [33]. After the reaction, the materials were abundantly washed with distilled water until reaching a neutral pH, leading to POL-OX@NiFe. Mass loss was calculated according to Eq. 2.

$$Mass\ loss\ (\%) = 1 - \frac{m_{CNT,w}}{m_{CNT}} \times 100 \quad (2)$$

in which $m_{CNT,w}$ is the mass of CNT after washing (in g) and m_{CNT} is the mass of CNT initially used (in g). POL-OX@NiFe was further thermally treated under inert atmosphere (N_2, 100 cm^3 min^{-1}) to remove the oxygenated moieties from its surface at 400 °C for 6 h (120 °C min^{-1}), leading to POL-400@NiFe.

2.2.3. Characterization

Part of the materials used in this work were thoroughly characterized in previous work [34]. The methodology used for characterization is described in supplementary information (Text S2).

2.3. Oxidative denitrogenation reactions

A quinoline (QN) solution ($[QN]_0^{oil} = 500$ mg L^{-1}, corresponding to $[N]_0^{oil} = 54$ mg L^{-1}) in 2,2,4-trimethylpentane was placed in a reaction vessel and heated to the desired temperature (50–80 °C). Then, a volume of H_2O_2 solution was added to reach the desired concentration ($[H_2O_2]_0$ = 1.23–123 g L^{-1}, oxidant-to-nitrogen molar ratio (O/N) of 2.3–230) at pH 1.0–11.0 (not buffered, adjusted with 0.5 M H_2SO_4 or 0.5 M NaOH), followed by the catalyst ([cat] = 0.25–5 g L^{-1}). The addition of the catalyst marked the beginning of the reaction ($t_0 = 0$ min). An oil-to-water (O/W) volume ratio of 80:20 was used in all experiments. Samples were periodically collected to monitor the concentration of QN in oil ($[QN]^{oil}$) and water ($[QN]^{water}$) phases using gas chromatography with flame ionization detection (GC-FID) and high-performance liquid chromatography (HPLC), respectively, as well as the concentration of H_2O_2 in the water phase using UV-Vis spectroscopy. Sampling of the reaction medium was carried out to maintain the original O/W ratio to preserve phase equilibria, ensuring that the total volume recovered during sampling did not exceed 10–15 vol% of the reaction medium. At

the end of the reaction, the catalyst was recovered from the reaction and dried overnight at 60 °C. Oil and water phases were stored separately. The total organic carbon (TOC) content of the water phase was also estimated. Non-catalytic (N.C.) experiment was conducted in the absence of catalyst. Previous works have shown that 2,24-trimethylpentane oxidation under similar conditions is negligible (<0.15 %) [5]. Adsorption runs were also considered in the oily phase only, following similar conditions as for the ODN reactions (80 °C, [adsorbent] = 2.5 g L^{-1}, $[QN]_0^{oil}$ = 500 mg L^{-1}). Tert-butanol (50 mM) and p-benzoquinone (10 mM) were used as scavengers for hydroxyl and superoxide radicals, respectively. Selected experiments were conducted in duplicate, and deviations were within ±5 %. Pyridine (PYR) was also considered as a model compound due to its higher barrier for oxidation [28]. The same procedure described above for QN was followed, with an initial PYR concentration of 305 mg L^{-1} (to achieve the same $[N]_0^{oil}$ of 54 mg L^{-1} used before) and hydrogen peroxide concentration of $[H_2O_2]_0$ = 12.3 g L^{-1} (equivalent to an O/N ratio of 23), 70 °C, pH_0 = 3.0 and [cat] = 2.5 g L^{-1}. A multi-component model fuel (containing QN and PYR) was also considered under the same conditions, with initial concentration of QN and PYR being adjusted to maintain the $[N]_0^{oil}$ equal to 54 mg L^{-1} ($[QN]_0^{oil}$ = 250 mg L^{-1} and $[PYR]_0^{oil}$ = 152.5 mg L^{-1}). Reusability tests were conducted with the multicomponent model fuel under the same operating conditions. After each reaction cycle, the catalyst was recovered and reused as obtained, without washing or regeneration, and no fresh catalyst was introduced.

2.3.1. Analytical methods

H_2O_2 concentration was determined using a colorimetric methodology based on the interaction between H_2O_2 and $TiOSO_4$ and measured using UV-Vis (UV–VIS Spectrometer, T70, PG Instrument Ltd., Lutterworth, UK) at 405 nm [35]. TOC was measured in a TOC-L (Shimadzu, Kyoto, Japan) equipment. QN and PYR concentration in the water phase ($[QN]^{water}$ and $[PYR]^{water}$) was followed by using a JASCO HPLC system (Hachioji, Japan). The separation of QN, PYR and reaction products was achieved with a mobile phase composed of acetonitrile **(A)** and ammonium acetate buffer solution (10 mmol) at pH 5.75 **(B)** and an Interchim Uptisphere Strategy Biphenyl (150 × 2.1 mm; 5 μm) column (Montluçon, France). The mobile phase was delivered at a 0.4 mL min^{-1} flow rate by a quaternary gradient pump (PU-2089). The mobile phase was initially fed at a proportion of 10 %:90 % (A:B) (from 0 to 7 min), then increased to 20 %:80 % (A:B) (maintained at this condition from 10 to 25 min), which was then returned to the initial condition (total running time of 32 min). Detection was achieved in a UV-Vis detector (UV-2075) at 313 nm for QN and 254 nm for PYR. QN concentration in the oily phase ($[QN]^{oil}$) during ODN reactions was followed in a GC-FID (Varian, model 3800, Palo Alto, California, USA) coupled with a SupelcoWax10 column (Bellefonte, Pennsylvania, USA). The oven temperature was set to 60 °C for 2 min, followed by a 10 °C min^{-1} ramp up to 210 °C (hold for 2 min), with helium as carrier gas under a 1 cm^3 min^{-1} flow. Detection was set to 200 °C and injection to 250 °C with a split ratio of 20. N-hexadecane was used as internal standard (1 mg mL^{-1}). During adsorption runs, QN concentration was estimated using UV-Vis at 313 nm. PYR concentration in the oil phase ($[PYR]^{oil}$) was estimated with an UV–VIS at 254 nm. QN and PYR data were plotted using normalized number of mols, and the calculations carried out for that are reproduced in Text S3. The kinetic model has been thoroughly described in a previous work of the group [5], and the information is reproduced in Text S4. Iron leaching was quantified in the aqueous phase using a colorimetric method reported elsewhere [36]. Carbon leaching from the CNT catalyst was estimated from TOC measurements after contact with H_2O_2 under acidic condition (pH_0 = 3, T = 80 °C, $[H_2O_2]_0$ = 123 g L^{-1}).

3. Results and discussion

3.1. Synthesis of materials and characterization

TEM images of POL-P@NiFe and POL-OX@NiFe can be seen in Fig. 1. Both materials display hollow tubular structures with multiple walls, including sections with straight walls (Fig. 1c) and sections with cup-stacked structures (Fig. 1b and f), indicating multiple growth events. This is typical from plastic-waste derived CNTs [7], as the cracking of the polymer fraction can yield distinct gases [37], which can influence the morphology of the obtained samples. Furthermore, since the CVD catalyst (NiFe) is composed by a mixture of distinct metallic particles, such as hematite, nickel ferrite and nickel oxide (Figure S1), it is also expected to influence the morphology of the CNTs obtained [7]. The outer diameter (Fig. 1d,h) obtained were 22.8 ± 0.6 and 28.2 ± 0.6 nm for POL-OX@NiFe and POL-P@NiFe, respectively, indicating that the harsh oxidation using HNO_3 resulted in the removal of outer layers from the CNT [38,39]. TEM analysis of the HNO_3-treated sample (POL-OX@NiFe) reveals occasional open or partially open CNT ends; however, as both closed and open ends coexist and TEM provides limited statistical representativeness, the acid treatment is primarily associated with outer-wall etching and surface functionalization rather than systematic tube-end opening.

The elemental composition of the CNTs is reported in Table 1. The content of oxygen is significantly higher for POL-OX@NiFe compared to POL-P@NiFe and POL-400@NiFe, which was expected given the HNO_3 oxidation treatment performed in sample POL-OX@NiFe. POL@NiFe also displays a high content of oxygenated moieties, which has been ascribed to oxygen transfer from the CVD catalyst during CNT growth, as reported elsewhere [40]. The content of iron and nickel significantly decrease upon acid washing.

The XRD patterns of the synthesized and post-treated materials are presented in Fig. 2. All samples exhibit a dominant reflection at around 26°, which is assigned to the (002) plane of graphitic carbon [41]. This reflection is characteristic of CNT-based materials and is consistent with previous reports on CNTs grown by CVD from polymeric carbon sources [42]. The diffractogram of the as-synthesized material, POL@NiFe (Fig. 2a), shows, in addition to the graphitic contribution, reflections assigned to alumina, cementite (Fe_3C), and nickel (Ni^0). The presence of Ni^0 confirms the reduction of the Ni-based catalyst under CVD conditions and is consistent with its role as the active phase for CNT growth [43]. The detection of cementite indicates partial carburization of iron during the high-temperature interaction with the carbon source, a phenomenon commonly observed in Fe-containing CNT catalysts [42].

Alumina reflections originate from the residual catalyst support. The purified sample POL-P@NiFe (Fig. 2b) still exhibits reflections associated with Ni^0 and Fe_3C, suggesting that acid treatment does not completely remove and carbide phases, likely due to partial encapsulation of these nanoparticles within the graphitic carbon structure, as confirmed by TEM. In contrast, the XRD pattern of POL-OX@NiFe (Fig. 2c) shows the absence of alumina reflections, which can be attributed to the aggressive nitric acid oxidation conditions employed. Despite this treatment, the graphitic (002) reflection remains clearly visible, indicating that the CNT structure is preserved. Metallic Ni^0 and cementite phases are still detected due to being embedded within the CNT framework or sufficiently protected from complete removal during oxidation. The interlayer spacing calculated from the (002) reflection using Bragg's law [44] falls in the range 0.336–0.340 nm for all samples, consistent with graphitic carbon typical of CNTs. Minor variations in d_{002} after purification and oxidation indicate limited changes in graphitic stacking without disruption of the CNT structure.

The surface functionalization induced by acid washing was assessed by FTIR spectroscopy (Figure S2). The spectrum of POL-OX@NiFe exhibits a pronounced band at around 1716 cm^{-1}, attributed to C═O stretching vibrations of carboxylic and carbonyl groups [45], confirming the introduction of oxygen-containing functionalities upon HNO_3

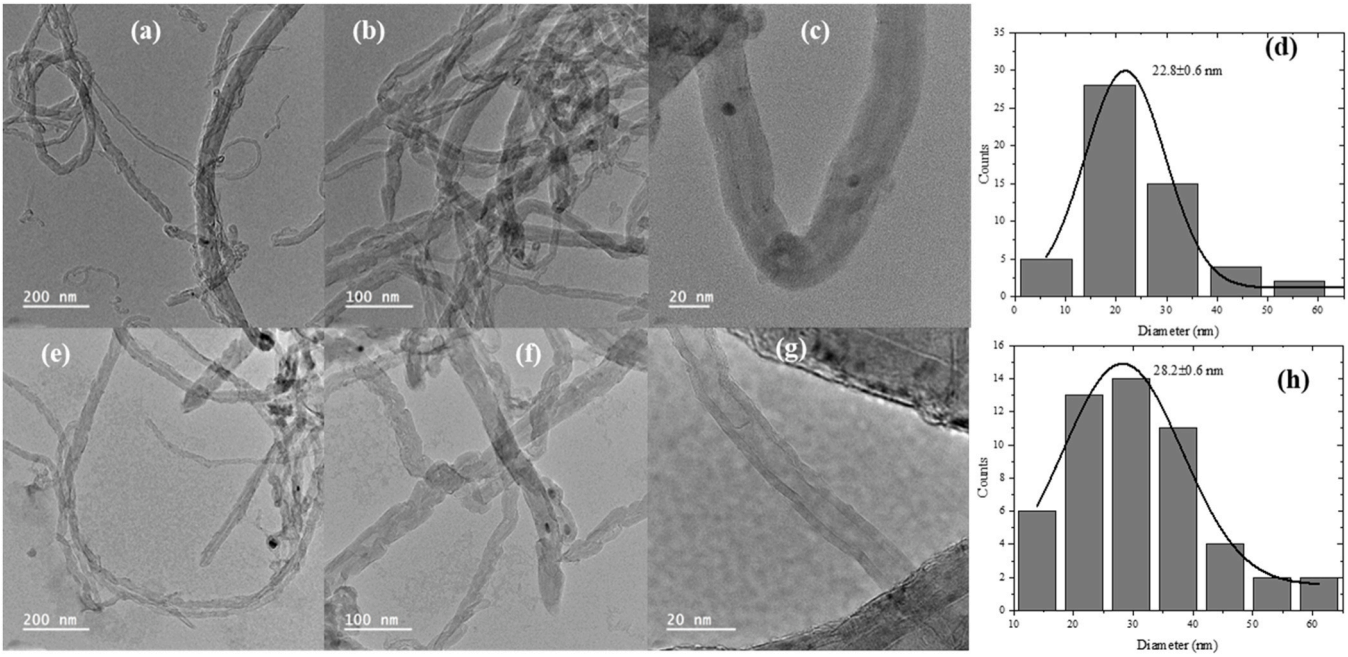

Fig. 1. TEM images of (a-c) POL-OX@NiFe and (e-g) POL-P@NiFe, and particle size distribution for (d) POL-OX@NiFe and (h) POL-P@NiFe.

Table 1
Elemental analysis of the CNTs.

Material	H/C	O/C	N/C	S/C	Fe (mg g^{-1})	Ni (mg g^{-1})
NiFe	-	-	-	-	88	49
POL@NiFe	0.0030	0.044	-	-	43	26
POL-P@NiFe	0.0004	0.010	-	0.0011	11	5
POL-OX@NiFe	0.0016	0.048	0.0012	-	7	3
POL-400@NiFe	0.0017	0.002	-	-	8	3

treatment. Additional bands observed in the 1170–1067 cm^{-1} region are assigned to C–O stretching modes of alcohol, ether, or ester groups [45]. In contrast, these features are significantly less intense or absent in the spectra of the less aggressively treated samples, indicating a lower degree of surface oxidation. The band at 1546 cm^{-1} was attributed to the stretching vibration of C═C from the backbone of the CNT [45]. These results are consistent with the elemental analysis and Raman spectroscopy data, confirming that nitric acid treatment primarily modifies the CNT surface chemistry without disrupting the graphitic structure.

A more extensive physicochemical characterization of the same CNT materials was reported in our previous work [34], in the present study, only a summary of the material's properties is reported and it can be found in the supplementary information (Table S1, Figure S3-S5). Briefly, the surface area of the samples (S_{BET}, Table S1 and Figure S3) increased upon acid washing, with harsher conditions (acid washing with HNO_3) resulting in higher surface areas (214 $m^2\ g^{-1}$) compared to milder washing conditions (148 $m^2\ g^{-1}$ from acid washing with H_2SO_4). The acid washing also affected the graphitization of the samples in a similar fashion (Figure S4): POL-OX@NiFe resulted in a D/G ratio of 0.99, whereas POL-P@NiFe and POL@NiFe resulted, respectively, in D/G ratios of 0.91 and 0.64, according to the results obtained in Raman spectroscopy. The results are consistent with previous reports [7,46]. Furthermore, in the HNO_3-treated material (POL-OX@NiFe), a peak centered at around 1620 cm^{-1} was observed (indicated with an arrow in Figure S4), which is ascribed to a more defective structure [47]. The materials demonstrated high oxidation resistance under air atmosphere (Figure S5), with the main event of mass loss happening at 640–650 °C for most materials. In N_2 atmosphere (Figure S5e), POL-OX@NiFe resulted in the highest mass loss, likely due to the removal of oxygenated moieties, consistent with elemental analysis results. The surface chemistry (Table S1) was also influenced by the acid washing, especially related to the introduction of basic moieties (25 *versus* 368 μmol g^{-1} of basic groups for POL-P@NiFe and POL-OX@NiFe, respectively), with further reduction upon heat treatment (63 μmol g^{-1} for POL-400@NiFe). A similar effect on the water contact angle (Table S1) was also observed: POL-OX@NiFe resulted in a lower value (117 ± 3°) compared to POL-P@NiFe (126 ± 2°) and all the remaining CNTs (>134°).

3.2. Screening of materials

The results regarding the screening of materials are displayed in Fig. 3. As it can be seen, the removal of QN (>50 % in 2 h of reaction) was more pronounced for the CNTs if compared to the non-catalytic run (N.C.) and with NiFe (ca. 10 % in 2 h of reaction for both) (Fig. 3a). Similarly, all CNTs resulted in a higher decomposition of hydrogen peroxide (>20 % in 2 h of reaction) compared to the N.C. run (ca. 5 % in 2 h of reaction) (Fig. 3b).

Among the catalysts tested, POL-OX@NiFe resulted in the fastest removal of QN from the oil phase (ca. 95 %), followed by POL-400@NiFe (54 %), POL@NiFe (24 %), POL-P@NiFe (13 %) and NiFe (10 %) in 1 h of reaction (Fig. 3a). The removal of QN from the oil phase seems to be positively influenced by the surface area (R^2 = 0.91, Figure S7a), with higher surface areas (POL-400@NiFe and POL-OX@NiFe) resulting in faster and higher removal rates. A different order of reactivity for the H_2O_2 decomposition was observed, in the order NiFe (87 %) > POL@NiFe (35 %) > POL-OX@NiFe (25 %) > POL-400@NiFe (14 %) > POL-P@NiFe (9 %) in 1 h of reaction·H_2O_2 decomposition seems to be associated with the O/C ratio of the CNT samples (R^2 = 0.88, Figure S7b). The apparent mismatch between hydrogen peroxide decomposition and QN removal arises because the initial H_2O_2 concentration largely exceeds the stoichiometric requirement for QN mineralization, and because oxidant decomposition alone does not determine effective oxidation. Adsorptive interaction between the catalyst surface and QN are crucial for effective utilization of the generated hydroxyl radicals [48]. As it can be seen in Figure S8,

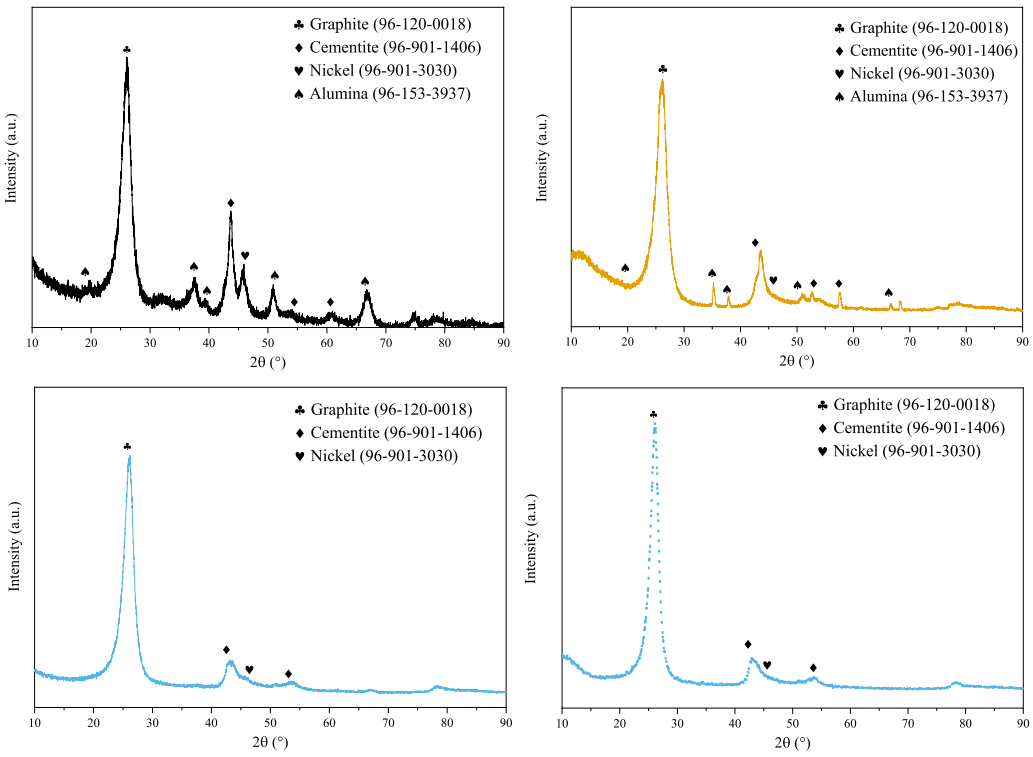

Fig. 2. XRD of (a) POL@NiFe, (b) POL-P@NiFe, (c) POL-OX@NiFe, and (d) POL-OX@NiFe recovered after a ODN reaction.

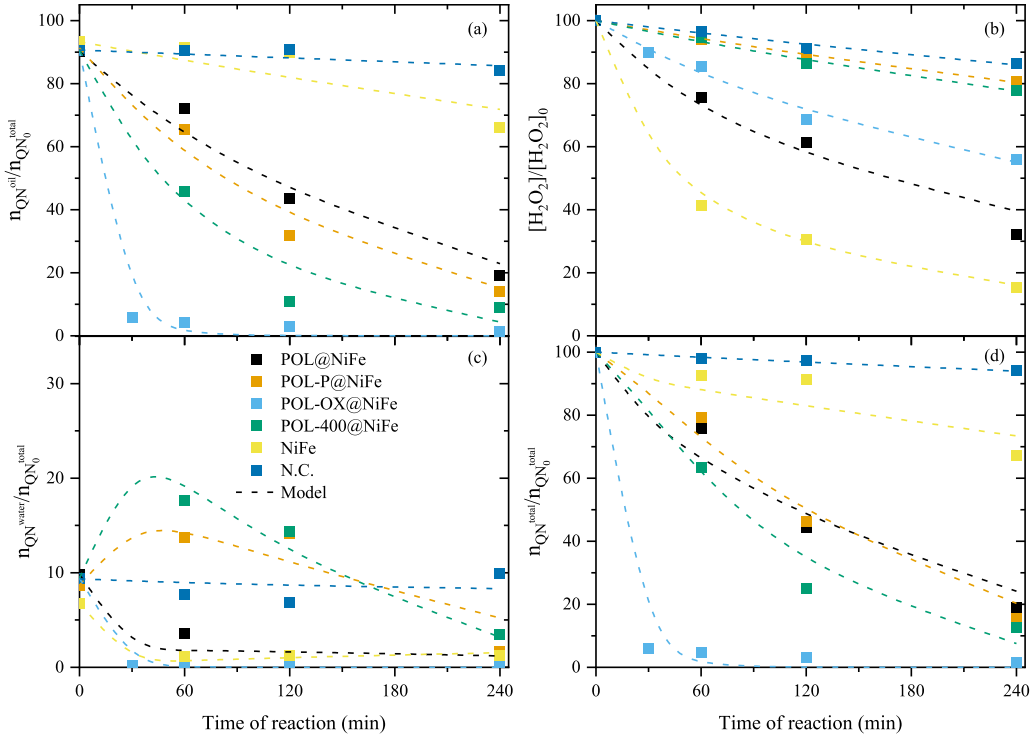

Fig. 3. Screening of materials. (a) Removal of QN from the model fuel phase, (b) decomposition of hydrogen peroxide in the aqueous phase, (c) QN in the water phase, and (d) overall QN abatement. (Conditions: $[QN]_0^{oil} = 500$ mg L^{-1} in 2,2,4-trimethylpentane, $[H_2O_2]_0 = 123$ g L^{-1} (O/N molar ratio = 230), O/W volume ratio = 80:20, T = 80 °C, [cat] = 2.5 g L^{-1}, pH of aqueous phase = 3.0). Dashed lines represent the kinetic model described in Text S4; parity plot shown on Fig. S6. Selected experiments were conducted in duplicate, with deviations within ±5 %.

POL-OX@NiFe displays a much higher adsorption capacity (ca. 28 %) for QN (in 2,2,4-trimethylpentane) compared to all remaining materials (5–9 %). The higher adsorption capacity allied to a more controlled H_2O_2 decomposition (Fig. 3b) is likely the reason behind its much higher activity towards the process. Unlike conventional supported catalysts, the CNTs evaluated in this work act as active catalytic materials,

contributing to both oxidant activation and pollutant adsorption, rather than serving as inert dispersing supports, as evidenced by their superior quinoline removal and hydrogen peroxide utilization efficiency compared to NiFe.

The concentration of QN in the water phase was also followed, and the results are depicted in Fig. 3c. In the presence of POL-OX@NiFe, QN is initially extracted from the oil phase and degraded in the water phase, not leading to any accumulation. The two materials with lower H_2O_2 decomposition ability (POL-P@NiFe and POL-400@NiFe) both result in an accumulation of QN in the water phase in the first hour of reaction, followed by its oxidation in the next 3 h of reaction. Nevertheless, neither of them allows complete QN conversion by the end of the 4 h of reaction. The decomposition of QN in the water phase seems to be associated with the O/C ratio of the CNT samples (R^2 = 0.98, Figure S7b). The non catalytic (N.C.) run results in a slight decomposition of QN in the first 1 h of reaction, followed by an increased concentration of QN in the water phase up to the end of reaction, due purely to extraction effect. The total abatement of QN, accounting for QN from both the oil and water phases, is shown in Fig. 3d. The profile is similar to the one observed for the removal of QN from the oil phase.

TOC conversion is displayed on Fig. 4, and it remains in the range of 16–31 %, with POL-OX@NiFe also resulting in a higher TOC removal compared to the remaining materials. The efficiency of hydrogen peroxide consumption was calculated. Higher rate of hydrogen peroxide decomposition (as seen for NiFe and POL@NiFe) resulted in lower efficiencies (2.0 and 2.7 %, respectively), whereas the materials with a more controlled decomposition resulted in higher efficiencies (8.1, 7.1, and 8.6 % for POL-P@NiFe, POL-OX@NiFe, and POL-400@NiFe, respectively). The N.C. resulted in a ca. 1.9 % efficiency. Nevertheless, the efficiencies are very low, and this makes sense because the concentration of hydrogen peroxide chosen for screening of catalysts was very high (ten times the needed concentration for QN mineralization, leading to a O/N molar ratio of 230). Leaching of iron and carbon were evaluated at the end of the reactions (Table S2). The CNT samples did not display any leaching (<LOD), whereas the metallic particles (NiFe) resulted in significant leaching (8.3 mg L^{-1}). Carbon leaching was not observed for any of the samples (Table S2). POL-OX@NiFe was chosen for optimization of the reaction conditions due to a higher activity towards the removal of QN via ODN in most parameters considered (removal and abatement of QN, TOC removal, and efficiency of hydrogen peroxide consumption).

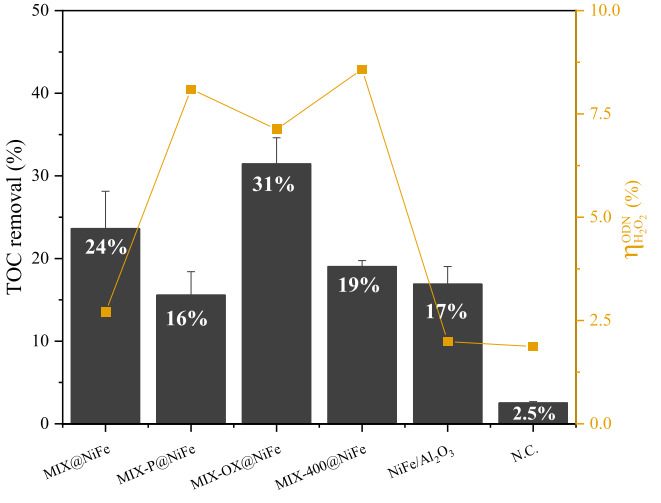

Fig. 4. TOC removal (left black Y-axis) and efficiency of hydrogen peroxide consumption (η_{H2O2}) (right yellow Y-axis) for the different CNT-based catalysts. (Conditions: $[QN]_0^{oil}$ = 500 mg L^{-1} in 2,2,4-trimethylpentane, $[H_2O_2]_0$ = 123 g L^{-1} (O/N molar ratio = 230), O/W volume ratio = 80:20, T = 80 °C, [cat] = 2.5 g L^{-1}, pH of aqueous phase = 3.0).

3.3. Optimization of reaction conditions

3.3.1. Effect of hydrogen peroxide concentration

Hydrogen peroxide concentration is a key parameter in ODN performance and one of the major contributors to the operational cost of peroxide-based processes [27]. Thus, the concentration of hydrogen peroxide was studied ranging from $[H_2O_2]_0$ = 123–1.2 g L^{-1} (O/N molar ratio 230–2.3), and the results are shown in Fig. 5. QN removal increased consistently with oxidant concentration: for ($[H_2O_2]_0 \geq$ 12 g L^{-1}), more than 90 % of QN was removed within 4 h, whereas the lowest concentration tested ($[H_2O_2]_0$ = 1.2 g L^{-1}) achieved only 60 % removal. Higher oxidant loadings also accelerated the initial reaction rate; at 30 min, QN removal exceeded 90 % and 80 % for $[H_2O_2]_0$ = 123 and 62 g L^{-1} (O/N = 230 and 115, respectively), while the stoichiometric amount required for mineralization ($[H_2O_2]_0$ = 12 g L^{-1}, O/N = 23) yielded 75 % removal in the same period. For sub-stoichiometric concentrations (<12 g·L^{-1}), most of the peroxide was consumed (>75 % in 4 h), whereas excess peroxide resulted in incomplete utilization, with only 40–50 % conversion for the highest concentrations (Fig. 5b). These results indicate that although higher oxidant concentrations enhance QN removal rates, they do so at the expense of lower oxidant utilization efficiency.

Fig. 5c shows the evolution of QN concentration in the aqueous phase. QN initially partitions into water, where it is rapidly degraded within the first 30 min for all conditions. At oxidant concentrations above $[H_2O_2]_0$ = 6 g L^{-1}, no significant accumulation of QN is detected in the water phase. In contrast, at the lowest oxidant loading ($[H_2O_2]_0$ = 1.2 g L^{-1}), QN persists and accumulates, leaving 0.13 μmol in the aqueous phase at the end of the reaction (16 % of the initial amount). Overall QN abatement (Fig. 5d) also depends strongly on the oxidant concentration: sub-stoichiometric conditions ($[H_2O_2]_0$ = 1.2 and 6 g L^{-1}) lead to incomplete conversion, achieving only 50 % and 95 % removal, respectively.

TOC removal was also strongly influenced by the initial hydrogen peroxide concentration (Figure S10a). Very high oxidant loadings ($[H_2O_2]_0$ = 123 and 62 g L^{-1}) result in poor efficiency of hydrogen peroxide consumption (ca. 7 % and 11 %, respectively). Similarly, the lowest concentration tested ($[H_2O_2]_0$ = 1.23 g L^{-1}) yielded an efficiency of only ~20 %. Intermediate concentrations ($[H_2O_2]_0$ = 6 and 12 g L^{-1}) performed better, with efficiencies of 30–40 %. Between $[H_2O_2]_0$ = 1.2–12 g L^{-1}, TOC removal increased proportionally with oxidant concentration (R^2 = 0.99, Figure S10b). However, further increasing the hydrogen peroxide concentration beyond 12 g L^{-1} no significant improvement in TOC abatement was produced.

Based on the results obtained, an initial hydrogen peroxide concentration of 12 g L^{-1} was selected as the best condition. At this loading, QN removal and abatement are both high after just 1 h of reaction (≈90 % and 85 %, respectively), while H_2O_2 degradation, utilization efficiency (η_{H2O2}) and TOC removal remain satisfactory (≈75 %, 40 %, and 29 %, respectively) compared with the other conditions evaluated.

3.3.2. Effect of catalyst concentration

Catalyst concentration was varied between 5 and 0.25 g L^{-1} , and the corresponding results are presented in Fig. 6. As expected, higher catalyst loadings accelerated both QN removal (Fig. 6a) and QN abatement (Fig. 6d). Catalyst concentration also had a strong influence on hydrogen peroxide consumption (Fig. 6b): only the highest dosage (5 g L^{-1}) enabled > 90 % H_2O_2 conversion. Catalyst loadings above 2.5 g L^{-1} achieved > 90 % QN removal within 1 h, whereas reducing the concentration to 1 g L^{-1} required an additional hour to reach equivalent removal. TOC removal (Figure S11) was similarly sensitive to catalyst concentration, increasing with loading and reaching a maximum of 37 % at 5 g L^{-1} . However, this highest dosage slightly decreased the hydrogen peroxide utilization efficiency compared with 2.5 g L^{-1} . Overall, while higher catalyst concentrations clearly enhance reaction performance, 2.5 g L^{-1} was selected as the best compromise between

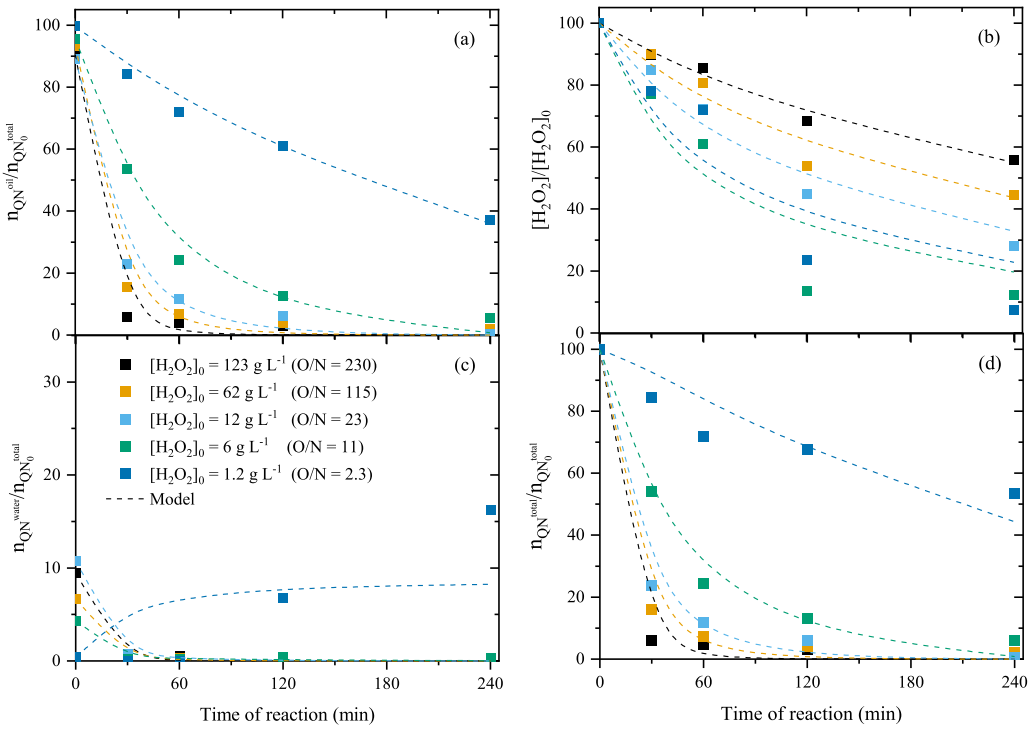

Fig. 5. ODN of QN with varying hydrogen peroxide concentration. (a) Removal of QN from the model fuel phase, (b) decomposition of H_2O_2, (c) QN in the aqueous phase and (d) overall abatement of QN. Conditions: $[QN]_0^{oil}$ = 500 mg L^{-1} in 2,2,4-trimethylpentane, $[H_2O_2]_0$ = 1.2–123 g L^{-1}, O/W volume ratio = 80:20, T = 80 °C, [POL-OX@NiFe] = 2.5 g L^{-1}, pH of aqueous phase = 3.0. Dashed lines represent the kinetic model described in Text S4, with kinetic constants obtained displayed in Table S3 and parity plot in Fig. S9. Selected experiments were conducted in duplicate, with deviations within ±5 %.

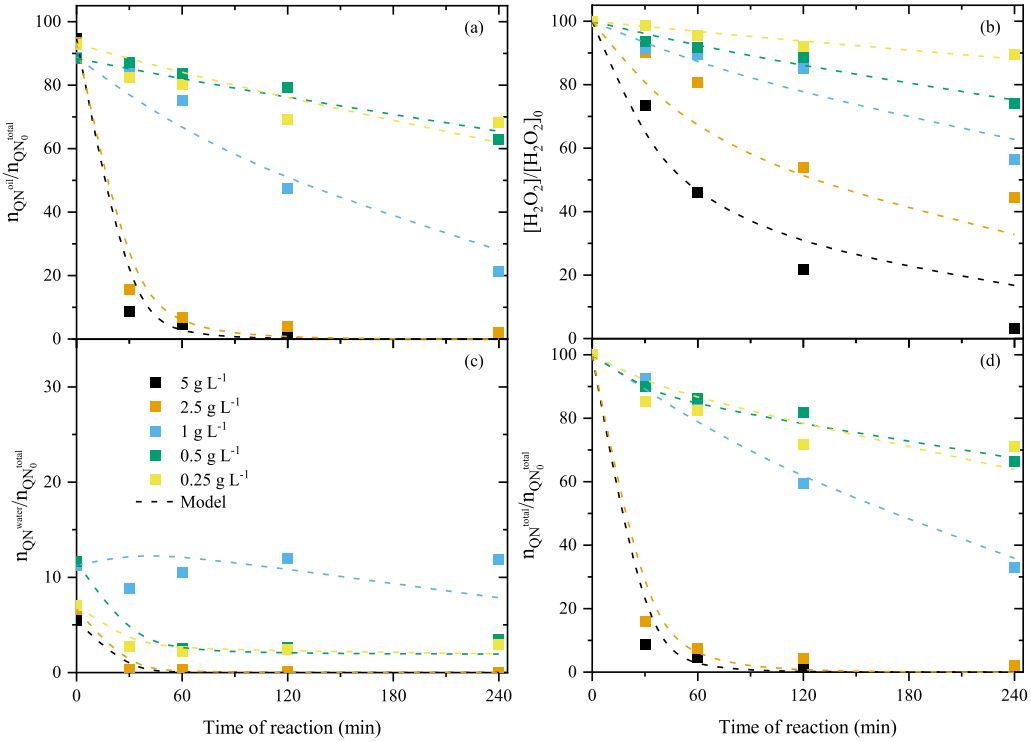

Fig. 6. ODN of QN with varying catalyst concentration. (a) Removal of QN from the model fuel phase, (b) decomposition of H_2O_2, (c) QN in the aqueous phase and (d) overall abatement of QN. Conditions: $[QN]_0^{oil}$ = 500 mg L^{-1} in 2,2,4-trimethylpentane, $[H_2O_2]_0$ = 12 g L^{-1}, O/W volume ratio = 80:20, T = 80 °C, [POL-OX@NiFe] = 0.25–5 g L^{-1}, pH of aqueous phase = 3.0. Dashed lines represent the kinetic model described in Text S4, with kinetic constants obtained displayed in Table S4, and parity plot in Fig. S12. Selected experiments were conducted in duplicate, with deviations within ±5 %.

activity and oxidant utilization.

3.3.3. Effect of the temperature

The results are presented in Fig. 7. At 50 °C, neither complete QN removal (Fig. 7a) nor full abatement (Fig. 7d) was achieved within 4 h, leaving ~200 mg L^{-1} of QN in the fuel and ~60 mg L^{-1} in the aqueous phase (33 % and 4 % of the initial amount, respectively). Increasing the temperature to 60 °C improved the process substantially, enabling ~90 % removal from the fuel phase within 4 h and preventing significant accumulation in water. At 70 °C and higher, > 90 % QN removal was reached within 2 h, with faster kinetics at increasing temperatures. These trends are consistent with previous findings for oxidation-based treatments in both aqueous [49] and biphasic systems [50]. Increasing the reaction temperature also enhanced TOC removal (Figure S13), reaching a maximum at 70 °C. At 80 °C, TOC abatement and hydrogen peroxide utilization efficiency both decreased, consistent with enhanced radical recombination and self-scavenging reactions at elevated temperatures [51–53]. Therefore, 70 °C was selected as the best reaction temperature.

3.3.4. Effect of the pH of aqueous phase

The effect of pH was evaluated in the range 1–11 using the previously optimized conditions for hydrogen peroxide ($[H_2O_2]_0$ = 12 g L^{-1}), catalyst concentration ([cat] = 2.5 g L^{-1}) and temperature (70 °C), and the results are reported in Fig. 8. QN removal from the oil phase was markedly faster under acidic conditions. At pH_0 = 1, more than 90 % of QN was removed within 30 min, whereas pH_0 = 3 required 120 min to achieve comparable removal, and pH values above 5 required at least 240 min. This enhanced performance at lower pH is directly linked to changes in QN solubility [54] and partition behavior [55] in response to aqueous-phase acidification. Previous studies report that QN solubility in water increases from 6.46 to 61.3 mg mL^{-1} as pH decreases from 3.07 to 0.55 [54]. Similarly, its partition coefficient shifts dramatically: above its pKa (4.9), QN remains largely in its neutral, lipophilic form, whereas at lower pH it becomes increasingly protonated and hydrophilic, with the partition coefficient approaching zero as pH approaches 0 [55]. Consequently, lower pH enhances mass transfer from the oil to the water phase, thereby promoting biphasic oxidation.

Despite its faster removal from the fuel phase, pH_0 = 1 led to significant accumulation of QN in the aqueous phase, peaking at 30 min (Fig. 8c). This behavior can be attributed to reduced H_2O_2 decomposition at pH 1 during the first 60 min (Fig. 8b). Because hydroxyl radical generation governs QN oxidation, limited hydrogen peroxide decomposition results in slower overall QN conversion (Fig. 8d). At higher pH values, particularly under basic conditions, QN removal decreased significantly (Fig. 8a). In these cases, 10–20 % of the initial QN mass (30–100 mg L^{-1}) remained in the oil phase by the end of the reaction. Hydrogen peroxide decomposition is less efficient at high pH [56], likely favoring pathways that lead to non-reactive species such as oxygen and water [49]. Consequently, QN also accumulated in the aqueous phase (Fig. 8c), reaching 180–340 mg L^{-1} (12–28 % of the initial amount), which resulted in lower overall abatement (Fig. 8d). TOC removal followed the same trend (Figure S16), with the highest efficiencies for hydrogen peroxide utilization observed at pH 3–5. In contrast, both TOC removal and hydrogen peroxide utilization efficiency dropped markedly at pH 1 and at pH values above 7.

The results reported here highlight the active role of the aqueous phase in governing ODN efficiency. Although water primarily acts as the extractant phase and carrier for H_2O_2 in the present biphasic ODN system, it also plays a critical role in governing reaction pathways and efficiency. The aqueous phase controls QN protonation and partitioning [55], thereby directly influencing mass transfer from the oil phase, particularly under acidic conditions. In addition, the pH of the water is highly correlated to hydroxyl radicals generation and recombination, thus affecting radical stability [57]. The observed dependence of denitrogenation performance on pH, temperature, and oxidant utilization efficiency therefore reflects not only intrinsic catalytic activity, but also the active role of the aqueous phase in regulating interfacial transport and oxidative pathways.

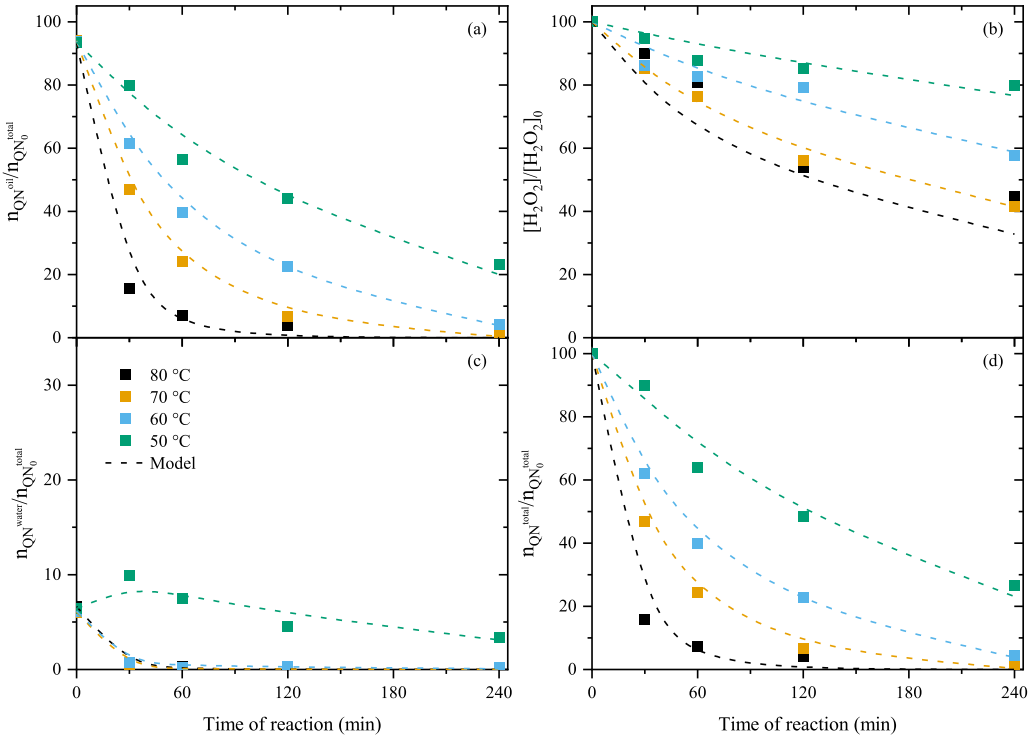

Fig. 7. ODN of QN with varying temperature. (a) Removal of QN from the model fuel phase, (b) decomposition of H_2O_2, (c) QN in the aqueous phase and (d) overall abatement of QN. Conditions: $[QN]_0^{oil}$ = 500 mg L^{-1} in 2,2,4-trimethylpentane, $[H_2O_2]_0$ = 12 g L^{-1}, O/W volume ratio = 80:20, T = 50–80 °C, [POL-OX@NiFe] = 2.5 g L^{-1}, pH of aqueous phase = 3.0. Dashed lines represent the kinetic model described in Text S4; parity plot in Fig. S14. Selected experiments were conducted in duplicate, with deviations within ±5 %.

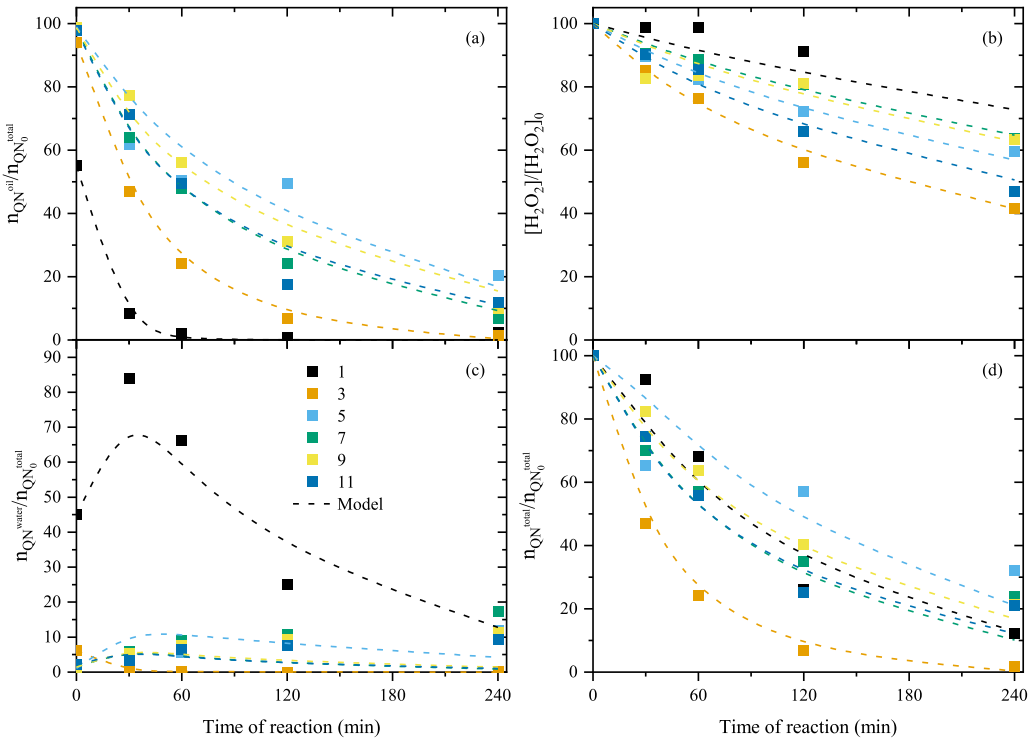

Fig. 8. ODN of QN with varying pH. (a) Removal of QN from the model fuel phase, (b) decomposition of H_2O_2, (c) QN in the aqueous phase and (d) overall abatement of QN. Conditions: $[QN]_0^{oil}$ = 500 mg L^{-1} in 2,2,4-trimethylpentane, $[H_2O_2]_0$ = 12 g L^{-1}, O/W volume ratio = 80:20, T = 70 °C, [POL-OX@NiFe] = 2.5 g L^{-1}, pH of aqueous phase = 1.0–11.0. Dashed lines represent the kinetic model described in Text S4, with kinetic constants obtained displayed in Table S5 and parity plot in Fig. S15. Selected experiments were conducted in duplicate, with deviations within ±5 %.

3.3.5. *Effect of initial concentration of QN*

The effect of the initial QN concentration was examined in the range 100–5000 mg L^{-1} using an O/N ratio of 23 (corresponding to $[H_2O_2]_0$ values between 2.4 and 120 g L^{-1}), a catalyst concentration of 2.5 g L^{-1}, a temperature of 70 °C, and an initial pH of 3.0. The results are shown in Fig. 9. For initial QN concentrations between 100 and 1000 mg L^{-1}, more than 90 % of QN was removed from the fuel phase within 60 min.

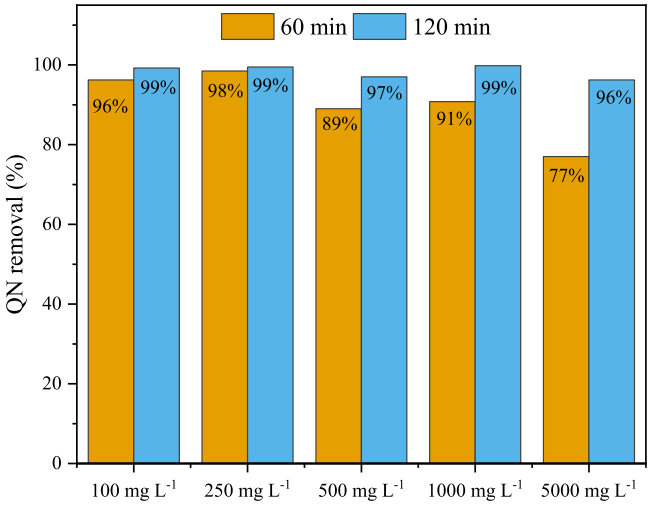

Fig. 9. ODN of QN with varying initial QN concentration. (a) Removal of QN from the model fuel phase, (b) decomposition of H_2O_2, (c) QN in the aqueous phase and (d) overall abatement of QN. Conditions: $[QN]_0^{oil}$ = 100–5000 mg L^{-1} in 2,2,4-trimethylpentane, $[H_2O_2]_0$ = 12 g L^{-1}, O/W volume ratio = 80:20, T = 70 °C, [POL-OX@NiFe] = 2.5 g L^{-1}, pH of aqueous phase = 3.0, 60–120 min of reaction. Selected experiments were conducted in duplicate, with deviations within ±5 %.

At the highest concentration tested (5000 mg L^{-1}), longer reaction times were required, with ~120 min needed to achieve > 90 % removal. Overall, effective QN removal was maintained across a wide range of initial concentrations, although higher loadings required longer reaction times.

3.4. *Kinetic modelling and insights*

Equations (S11), (S14) and (S15), described in Text S4, were fitted to the experimental data, resulting in the kinetic parameters displayed in Tables 2, 3, S2-S4, and S6. The model exhibited an excellent fit, as indicated by the high determination coefficients (R^2 > 0.955), low residual errors (SSE_{model} < 0.097), and good agreement between predicted and experimental values, as demonstrated by parity plots (Figures S7, S10, S13-14, S16, S19) and the model curves (dashed lines) shown in Figures 3–8 and S18.

For screening experiments, the apparent rate constants for H_2O_2 decomposition followed the order NiFe > POL@NiFe > POL-OX@NiFe > POL-400@NiFe ~ POL-P@NiFe > N.C. All CNT-containing catalysts significantly enhanced the mass transfer of quinoline (QN) from the oil to the aqueous phase, as reflected in much higher $k'_{QN,mt}$ values (0.34–5.32 h^{-1}) compared to the non-catalytic run (0.01 h^{-1}). The CVD catalyst (NiFe) showed only a minor effect (0.07 h^{-1}). This enhancement suggests that CNTs act as phase-transfer catalysts, promoting interfacial diffusion between the immiscible phases. Among them, POL-OX@NiFe exhibited the highest $k'_{QN,mt}$ and the greatest apparent oxidation coefficient $k'_{QN,ox}$, which correlated strongly with the surface basic group density of the CNTs (R^2 = 0.96, Figure S17). The large difference in magnitude $k'_{QN,ox} >> k'_{QN,mt}$ indicates that the process is mass-transfer-limited, emphasizing the critical role of CNTs in facilitating phase transfer and efficient oxidant utilization.

Results from kinetic modeling studies in the literature are summarized in Table S6. Only one previous work has developed a biphasic kinetic model that simultaneously accounts for hydrogen peroxide

Table 2
Kinetic and statistical coefficients obtained for each material during ODN.

Coefficient	POL@NiFe	POL-P@NiFe	POL-OX@NiFe	POL-400@NiFe	NiFe	N.C.
k'_{H2O2} (mol^{-1} h^{-1})	5.29	0.90	2.86	0.98	12.30	0.58
$k'_{QN,mt}$ (h^{-1})	0.34	0.47	5.32	0.84	0.07	0.01
$k'_{QN,ox}$ ($kmol^{-1}$ h^{-1})	0.233	0.031	1.778	0.028	0.167	0.002
POW	0.18					
SSE_{model}	0.018	0.011	0.004	0.013	0.013	0.002
R^2	0.989	0.994	0.999	0.992	0.993	0.999

Table 3
Kinetic and statistical coefficients obtained for each temperature during ODN.

Coefficient	50 °C	60 °C	70 °C	80 °C
k'_{H2O2} (mol^{-1} h^{-1})	12.31	25.83	52.00	70.29
$k'_{QN,mt}$ (h^{-1})	0.40	0.80	1.36	2.47
$k'_{QN,ox}$ ($kmol^{-1}$ h^{-1})	0.59	12.54	61.41	14.58
POW	0.18			
SSE_{model}	0.011	0.008	0.001	0.008
R^2	0.995	0.996	0.999	0.996

consumption, mass transfer, and pollutant oxidation [11], although the operating conditions and pollutants were quite different. In our earlier study on the ODN of quinoline using Fe-derived CNTs [5], the apparent rate constants for H_2O_2 decomposition ($k'_{H2O2} = 1.3–10.2$ mol^{-1} h^{-1}) and mass transfer ($k'_{QN,mt} = 0.5–2.1$ h^{-1}) were comparable to those obtained here, while the oxidation coefficients ($k'_{QN,ox} = 0.0127–0.0665$ $kmol^{-1}$ h^{-1}) fell within the lower end of the range determined in the present work (0.028–1.778 $kmol^{-1}$ h^{-1}). Most other kinetic studies on ODN and related oxidation reactions employ simplified pseudo–first-order models [18,58–62] or adsorption–desorption approaches [63], which do not account for biphasic mass-transfer effects. As a result, direct comparison with the kinetic model used in this work is limited.

The kinetic parameters obtained at 50–80 °C (Table 3) confirmed a strong temperature dependence for all steps, particularly for H_2O_2 decomposition. QN oxidation increased steadily up to 70 °C but decreased at 80 °C, consistent with excessive radical formation leading to recombination or self-scavenging [51–53]. This behavior mirrors the trends observed for TOC removal and oxidant utilization, indicating that 70 °C provides the optimal balance between radical generation and stability.

Activation energies were estimated from Arrhenius plots (Figure S18) and are listed in Table 4. The apparent activation energy for H_2O_2 decomposition (56 kJ mol^{-1}) agrees well with reported values for aqueous Fenton and CWPO systems (45–89 kJ mol^{-1} [64,65]). In contrast, the activation energy for QN oxidation (214.6 kJ mol^{-1}) is substantially higher, which can be attributed to the additional energy barrier imposed by interfacial mass transfer in the biphasic system. Reported activation energies for homogeneous quinoline oxidation using H_2O_2 are much lower (22–23 kJ mol^{-1} [66,67]), while other QN degradation systems were reported in the range 29–93 kJ mol^{-1} [68–71]. Values reported for the oxidative denitrogenation of related nitrogen-containing compounds, such as indole (26.6 [59] and 31.1 kJ mol^{-1} [61]), pyridine (27.5 kJ mol^{-1} [60]), and carbazole (69.3 kJ mol^{-1} [62]) are also significantly lower. It should be noted, however, that these works employed simplified pseudo-first-order models that neglect mass transfer limitations inherent to biphasic systems. Therefore, direct comparison with the present results is not straightforward, as the higher apparent E_a observed here reflects both chemical and interfacial transport contributions explicitly considered in the current kinetic formulation.

Table 4
Activation energy and pre-exponential factor.

Coefficient	Pre-exponential factor (mol^{-1})	E_a (kJ mol^{-1})	R^2	SSE_{model}	Range
k'_{H2O2} (mol^{-1} h^{-1})	$5.73E^{-11}$	56.4	0.978	0.003	50–80 °C
$k'_{QN,mt}$ (h^{-1})	$1.58E^{-09}$	56.8	0.998	0.041	50–80 °C
$k'_{QN,ox}$ ($kmol^{-1}$ h^{-1})	$2.75E^{-38}$	214.6	0.974	0.294	50–70 °C

Figure S19 further supports the interpretation through radical-scavenger experiments. In the absence of scavengers, QN removal surpassed 90 % in 2 h of reaction. The addition of tert-butanol (50 mM) caused a pronounced decrease in QN oxidation rate in both phases, reducing global removal after 2 h from ca. 90 % to ~40 % strongly suggesting that hydroxyl radicals ($HO^{\bullet}$) are the dominant oxidizing species under the studied conditions. The addition of p-benzoquinone (10 mM) caused a milder inhibition (QN removal at 2 h of ~66 %), indicating that superoxide radicals ($O_2^{\bullet-}$) participate as secondary oxidants. The transient accumulation of quinoline in the aqueous phase (Figure S19c) reflects its extraction from the organic phase followed by subsequent oxidation, consistent with the biphasic kinetic model that accounts for interfacial mass transfer. The model curves (dashed lines) reproduce well the observed scavenging trends (supported by parity plots in Figure S20), and the oxidation rate constant (shown on Table S7) decreases markedly when $HO^{\bullet}$ or $O_2^{\bullet-}$ are quenched.

In addition to kinetic modeling and radical scavenger experiments, the formation of transient oxidation intermediates was qualitatively observed during the reaction. Time-resolved chromatographic monitoring of the aqueous phase revealed the appearance of two signals (RT = 2.1 and 8.3 min) that were absent at the beginning of the reaction, increased in intensity at intermediate reaction times, and subsequently decreased as the reaction progressed (Figure S21). The transient evolution of these signals is consistent with the formation and consumption of intermediate species during ODN. However, due to the lack of complementary mass spectrometric or NMR data, these intermediates could not be structurally identified, and their discussion is therefore limited to a qualitative level.

Collectively, the kinetic and scavenging analyses support the interpretation that (i) QN oxidation is primarily driven by $HO^{\bullet}$ radicals generated via catalytic H_2O_2 decomposition, (ii) $O_2^{\bullet-}$ species play a secondary but synergistic role, and (iii) the process efficiency is strongly influenced by mass transfer between the oil and aqueous phases, where CNTs act as interfacial promoters enhancing oxidant utilization. The proposed pathway is intended as a qualitative representation of QN oxidation under ODN conditions, based on previously reported reaction routes [21–23], rather than a comprehensive identification of reaction intermediates.

3.5. Other nitrogenated compounds and reutilization of POL-OX@NiFe

The ODN of PYR was evaluated under the optimized conditions identified for QN, both as a single-component fuel and in a mixed system with QN (Fig. 10). When PYR was treated as the sole nitrogen-containing compound, its removal was significantly slower than that observed for QN, consistent with its higher resistance to oxidation [28]. PYR removal

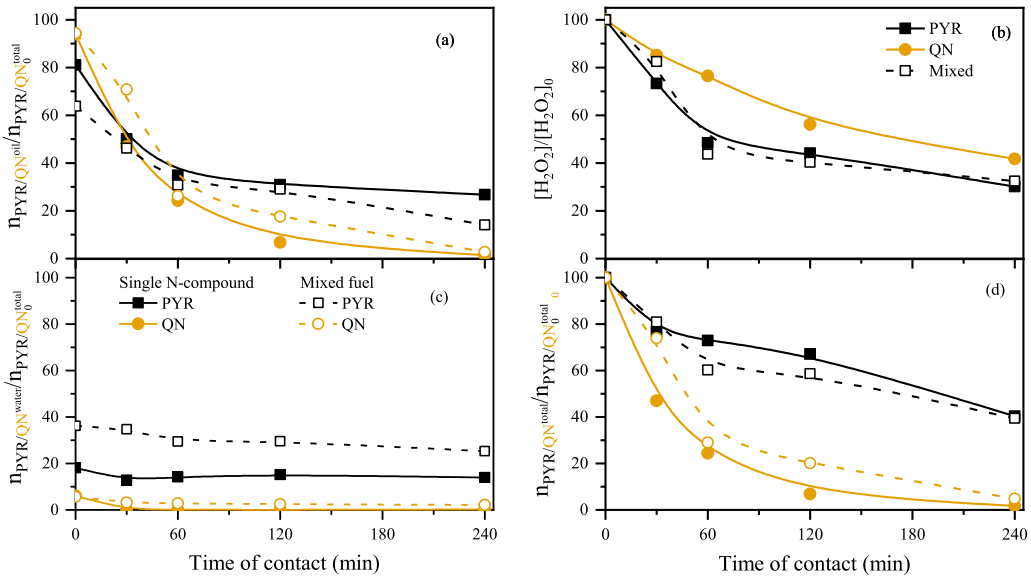

Fig. 10. ODN of PYR, QN and a mixed fuel containing both N-compounds. (a) Removal of PYR or QN from the model fuel phase, (b) decomposition of H_2O_2, (c) PYR or QN in the aqueous phase and (d) overall abatement of PYR or QN. Conditions: $[N]_0^{oil} = 54$ mg L^{-1} in 2,2,4-trimethylpentane, $[H_2O_2]_0 = 12$ g L^{-1}, O/W volume ratio = 80:20, T = 70 °C, [POL-OX@NiFe] = 2.5 g L^{-1}, pH of aqueous phase = 3.0. Selected experiments were conducted in duplicate, with deviations within ±5 %. Lines are only intended to guide the eyes.

from the model fuel achieved around 75 % in 4 h of reaction, and total abatement of 60 %. In the mixed QN–PYR system, QN was preferentially removed. PYR oxidation was not significantly affected compared to single-PYR case, with a slight increase in the removal of PYR from the model fuel (ca. 85 %) compared to the single-component case. This behavior suggests competitive effects, likely arising from preferential adsorption and oxidation of the more reactive QN, which consumes reactive oxygen species and limits their availability for PYR oxidation. Partial PYR conversion was still achieved (60 %, Fig. 10d), indicating that the optimized ODN conditions retain activity toward more recalcitrant nitrogen-containing compounds, albeit with reduced efficiency. TOC removal and efficiency of H_2O_2 utilization (Figure S22) were lower for PYR and for the multi-component system compared to pure QN experiments. Overall, these results highlight that while the proposed system is highly effective for QN removal, the oxidation of simpler, more oxidation-resistant nitrogen heterocycles such as PYR remains more challenging.

The reusability of the POL-OX@NiFe catalyst was evaluated using the multicomponent model fuel under identical operating conditions (Fig. 11). Clear changes in reaction profiles were observed upon catalyst reutilization. In particular, the removal profiles from the model oil phase and the overall abatement curves show a noticeable deviation from the first run, with the effect being more pronounced for PYR than for QN. A significant alteration in hydrogen peroxide decomposition was observed

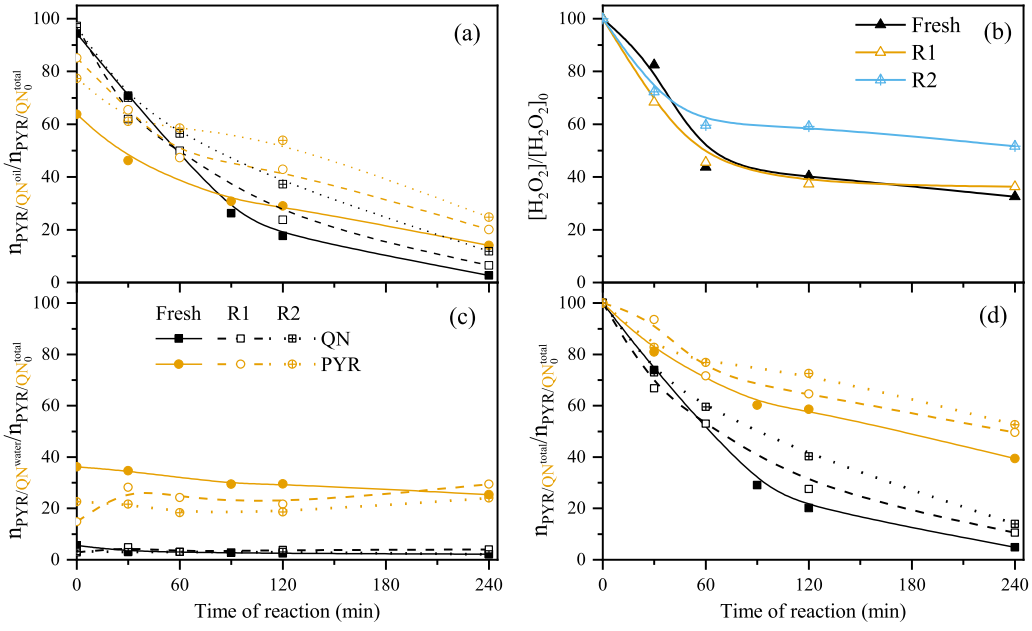

Fig. 11. Reutilization runs of multicomponent model fuel containing both QN and PYR. (a) Removal of PYR or QN from the model fuel phase, (b) decomposition of H_2O_2, (c) PYR or QN in the aqueous phase and (d) overall abatement of PYR or QN. Conditions: $[N]_0^{oil} = 54$ mg L^{-1} in 2,2,4-trimethylpentane, $[H_2O_2]_0 = 12$ g L^{-1}, O/W volume ratio = 80:20, T = 70 °C, [POL-OX@NiFe] = 2.5 g L^{-1}, pH of aqueous phase = 3.0. Lines are only intended to guide the eyes.

between the first and second runs, with a markedly slower consumption of H_2O_2 after reuse. This change suggests a modification of the catalyst surface during the initial reaction cycle, likely due to partial coverage by adsorbed reaction intermediates or by-products, which reduces the availability of active sites for oxidant activation. As a consequence, the generation of reactive oxygen species is diminished, directly impacting the oxidation kinetics, particularly for the more oxidation-resistant PYR. The stronger loss of activity toward PYR compared to QN highlights the greater sensitivity of recalcitrant nitrogen-containing compounds to changes in catalyst surface chemistry and oxidant availability. These results indicate that although the catalyst remains active after reuse, surface regeneration strategies may be required to maintain optimal oxidant activation and performance toward more resistant nitrogen species.

The sample recovered after catalytic experiments was analysed by XRD (Fig. 2d) and shows no significant modification in its overall diffraction pattern when compared to POL-OX@NiFe (Fig. 2c). The persistence of the graphitic (002) reflection and the same set of reflections associated with Ni^0 and Fe_3C indicate that no major phase transformation occurs during the catalytic run, supporting the structural stability of the material under the reaction conditions. The absence of detectable changes in the XRD patterns indicates that the observed loss of catalytic activity upon reuse is not associated with bulk structural degradation or phase transformation of the CNT structure or the embedded metallic species. Complementary FTIR analysis of the recovered material (Figure S2) reveals subtle changes in surface chemistry, notably a shift of a band from ~1170 to ~1067 cm^{-1} after reaction, which indicates a modification of the chemical environment of oxygen-containing functional groups during ODN; or may indicate the adsorption of N-containing molecules [45]. These surface changes arise from interaction of oxygenated groups with reactive oxygen species or oxidation intermediates, leading to partial transformation or deactivation of surface functionalities involved in oxidant activation. These surface-level modifications, while not detectable by bulk-sensitive techniques such as XRD, highlight the need for strategies aimed at preserving or regenerating surface-active sites, such as mild post-reaction treatments, controlled surface re-oxidation to maintain catalytic activity over extended reuse cycles, particularly for more oxidation-resistant nitrogen-containing compounds.

3.6. Comparison with literature

Table 5 summarizes oxidative denitrogenation systems employing carbon-based catalysts. Reported denitrogenation efficiencies range from 0 % to 100 %, with reaction temperatures between 25 and 100 °C, catalyst concentrations of 0.5–3.33 g L^{-1} , O/N molar ratios from 0 to 820, acidic pH values (3–6), and fuel-to-extractant volume ratios between 99:1 and 50:50. Only one study [4] employed carbon materials purely as catalysts for ODN, rather than as supports or in hybrid systems, and only two works reported waste-derived materials to produce the catalysts [23,24]. In the present work, we synthesized oxygen-doped CNTs from simulated plastic waste, achieving > 89 % QN removal within 1 h using a relatively low O/N ratio of 23, which is lower than most previous reports (only two studies used O/N < 23 [18,58]). The main limitation of this approach is the slightly higher reaction temperature required (70 °C) compared with most studies using hydrogen peroxide (25–60 °C).

4. Conclusions

This study investigated the oxidative denitrogenation (ODN) of a model fuel, composed of quinoline (QN) and 2,2,4-trimethylpentane, in biphasic systems using carbon nanotubes (CNTs) derived from polyolefin mixtures over a $NiFe/Al_2O_3$ catalyst. The POL-OX@NiFe catalyst exhibited superior performance, achieving > 89 % QN removal in just 1 h, while ensuring controlled hydrogen peroxide decomposition, enhanced adsorption capacity, and improved phase-transfer. Best-performing conditions were identified as $[H_2O_2]_0$ = 12 g L^{-1} (O/N = 23) for $[QN]^{oil}_0$ = 500 mg L^{-1} , catalyst loading of 2.5 g L^{-1} , temperature of 70 °C, and initial pH of 3.0. Under these conditions, TOC reduction reached 35 % and hydrogen peroxide utilization efficiency (η_{H2O2}) was 77 %.

Kinetic analysis revealed mass transfer as the rate-limiting step, with POL-OX@NiFe significantly enhancing QN mass transfer ($k'_{QN,mt}$ =

Table 5
Reports in the literature for ODN using carbon-containing materials as catalysts.

Fuel	Catalyst	Extractant	Operational Conditions	QN removal	Ref.
QN in Toluene (C_0 = 50 ppm)	Fe_2O_3/C	Aqueous H_2O_2 phase	$V_{fuel}/V_{extractant}$ = 99:1, [cat] = 1 g L^{-1}, O/N = 112, T = 25 °C, pH = 4.0, t = 3 h.	60 % removal	[21]
QN in Cyclohexane ($[N]_0$ = 50 ppm)	Fe/C and FeMo/C	Aqueous H_2O_2 phase	$V_{fuel}/V_{extractant}$ = 5:1, [cat] = 2.5 g L^{-1}, O/N = 495, T = 25 °C, pH = 4.0, t = 2 h.	100 % removal	[22]
QN in Cyclohexane ($[N]_0$ = 30 ppm)	N-Doped CNT/red mud	Aqueous H_2O_2 phase	$V_{fuel}/V_{extractant}$ = 5:1, [cat] = 3.33 g L^{-1}, O/N = 820, t = 45 min.	80 % removal	[23]
QN in Cyclohexane (C_0 = 500 ppm)	WEEE-clay hybrid material	ACN	$V_{fuel}/V_{extractant}$ = 10:2, O/N = 72, T = 60 °C, t = 3 h.	Removal rate of 73.5 mg_{QN} g_{cat}^{-1}	[24]
QN in n-Octane (C_0 = 5000 ppm)	TiO_2@C	Acetic Acid	$V_{fuel}/V_{extractant}$ = 20:2 [cat] = 0–0.5 g L^{-1}, O/N = 0–15, T = 30–50 °C, 100–1000 rpm, 5–10 wt% water, t = 2 h.	0 % removal	[58]
QN in Cyclohexane (C_0 = 500 ppm)	C/red mud	Aqueous H_2O_2 Phase	$V_{fuel}/V_{extractant}$ = 5:1, [cat] = 3.33 g L^{-1}, O/N = 450, t = 1 h.	100 % removal	[25]
QN in Toluene (C_0 = 25 ppm)	Fe/Onion-like Carbon	Aqueous H_2O_2 Phase	V_{fuel} = 10 mL, [cat] = 1 g L^{-1}, C_{H2O2} = 0.05 mol L^{-1}, T = 25 °C, pH 6.	93 % removal	[72]
QN in Cyclohexane ($[N]_0$ = 500 ppm)	FeMo/CNT	Aqueous H_2O_2 Phase	$V_{fuel}/V_{extractant}$ = 5:1, [cat] = 3.33 g L^{-1}, O/N = 50, t = 50 min.	100 % removal	[26]
QN in n-octane* (C_0 = 1000 ppm)	W_2N@C	Acetic acid	$V_{extractant}$ = 2 mL, m_{cat} = 5 mg, O/N = 10, T = 37 °C, U.S. = 40 %, t = 2 h.	90 % removal	[18]
QN in n-dodecane (C_0 = 500 ppm)	O, P-co-doped carbon	Acetic acid	$V_{fuel}/V_{extractant}$ = 10:10, [cat] = 3 g L^{-1}, 50 mL min^{-1} of O_2, T = 100 °C, t = 4 h	86 % removal	[59]
QN in 2,2,4-trimethylpentane (C_0 = 1000 ppm)	CNT@Fe	Aqueous H_2O_2 Phase	$V_{fuel}/V_{extractant}$ = 80:20, [cat] = 2.5 g L^{-1}, O/N = 230, T = 80 °C, pH = 3.0, t = 1 h.	98 % removal	[5]
QN in 2,2,4-trimethylpentane (C_0 = 100–5000 ppm)	CNT@NiFe	Aqueous H_2O_2 Phase	$V_{fuel}/V_{extractant}$ = 80:20, [cat] = 2.5 g L^{-1}, O/N = 23, T = 70 °C, pH = 3.0, t = 1 h.	89–97 % removal of QN depending on the concentration	This work

3.09 h^{-1}) compared with other CNTs (0.34–0.83 h^{-1}) and the non-catalytic system (0.01 h^{-1}). Activation energies for QN oxidation and hydrogen peroxide decomposition were estimated at 214 and 59 kJ mol^{-1} , respectively. Scavenging tests strongly suggest that hydroxyl radicals are the primary reactive species involved in QN oxidation under the studied conditions.

Beyond denitrogenation performance, the sustainability of the proposed ODN system is supported by quantitative indicators, including high hydrogen peroxide utilization efficiency, measurable TOC abatement, operation under mild conditions (70 °C, atmospheric pressure), and the use of polymer-derived CNTs representative of waste-derived carbon catalysts. These metrics provide a quantitative basis for sustainability assessment aligned with green chemistry principles, particularly waste valorization, energy efficiency, and controlled oxidant utilization.

It should be noted that the interpretation proposed herein is based on kinetic analysis and radical scavenging experiments and therefore provides a qualitative description of the dominant oxidation pathways; direct identification of reactive oxygen species, oxidation intermediates, and a complete nitrogen mass balance were beyond the scope of the present work. While nitrogen removal was assessed through QN disappearance, aqueous-phase conversion, and TOC abatement, the detailed distribution of nitrogen among oxidized organic intermediates, inorganic nitrogen species, or surface-associated forms was not resolved. Additionally, although the catalyst retained its bulk structural integrity upon reuse, partial loss of activity was observed and is attributed to surface-level modifications during reaction, highlighting the need for further strategies to preserve or regenerate active surface functionalities over extended operation. Although QN and PYR are widely used model compounds, the behavior of real fuels may differ due to their complex composition. Future work will address product and nitrogen speciation and validate catalyst performance in real fuel matrices.

CRediT authorship contribution s

Fernanda F. Roman: Writing – original draft, Visualization, Methodology, Investigation, Formal analysis, Data curation, Conceptualization. **Adriano S. Silva:** Writing – original draft, Visualization, Formal analysis, Data curation. **Jose L. Diaz de Tuesta:** Writing – review & editing, Project administration, Methodology, Funding acquisition, Conceptualization. **Adrián M.T. Silva:** Writing – review & editing, Supervision. **Joaquim L. Faria:** Writing – review & editing, Supervision. **Helder T. Gomes:** Writing – review & editing, Supervision, Project administration, Funding acquisition.

Declaration of Competing Interest

The authors declare that they have no known competing financial interests or personal relationships that could have appeared to influence the work reported in this paper.

Acknowledgements

This work was supported by national funds through FCT/MCTES (PIDDAC): CIMO UID/00690/2025 (10.54499/UID/00690/2025) and UID/PRR/00690/2025 (10.54499/UID/PRR/00690/2025); SusTEC, LA/P/0007/2020 (DOI: 10.54499/LA/P/0007/2020). This research was also supported by Fundação para a Ciência e a Tecnologia, I.P. /MCTES through national funds: LSRE-LCM, UID/50020/2025; and ALiCE, LA/P/0045/2020 (DOI: 10.54499/LA/P/0045/2020). Fernanda F. Roman acknowledges the national funding by FCT and the European Social Fund, FSE, through the individual research grant SFRH/BD/143224/2019. Adriano S. Silva thanks the financial support from FCT under MIT Portugal Program with Ph.D. grant SFRH/BD/151346/2021. J. L. Diaz de Tuesta acknowledges the research grant (2022-T1/AMB-23946) by the program of Atracción al Talento of Comunidad de Madrid (Spain). The authors are grateful to *Sociedade Ponto Verde* for the financial support through the project "*Estudo técnico-económico para a valorização de resíduos de embalagens plásticas em nanotubos de carbono*."

Appendix A. Supporting information

Supplementary data associated with this article can be found in the online version at doi:10.1016/j.jece.2026.121864.

Data availability

The dataset is available at a data repository

Dataset for paper "Oxidative denitrogenation using sustainable carbon nanotubes: Effect of reaction conditions on hydrogen peroxide efficiency" (Dataverse)

References

[1] F.F. Roman, J.L. Diaz de Tuesta, A.M.T. Silva, J.L. Faria, H.T. Gomes, Carbon-based materials for oxidative desulfurization and denitrogenation of fuels: a review, Catalysts 11 (2021) 1239, https://doi.org/10.3390/catal11101239.
[2] P. Grennfelt, A. Engleryd, M. Forsius, O. Hov, H. Rodhe, E. Cowling, Acid rain and air pollution: 50 years of progress in environmental science and policy, Ambio 49 (2020) 849–864, https://doi.org/10.1007/s13280-019-01244-4.
[3] S. Kwao, S. Vedachalam, A.K. Dalai, J. Adjaye, Review of current advances in hydrotreating catalyst support, J. Ind. Eng. Chem. 135 (2024) 1–16, https://doi.org/10.1016/j.jiec.2024.01.027.
[4] R.G. Faria, D. Silva, F. Mirante, S. Gago, L. Cunha-Silva, S.S. Balula, Advanced technologies conciliating desulfurization and denitrogenation to prepare clean fuels, Catalysts 14 (2024) 137, https://doi.org/10.3390/catal14020137.
[5] F.F. Roman, Ld.G. Piccinin, A.S. Silva, J.L. Diaz de Tuesta, A. Vieira, A.M.T. Silva, J.L. Faria, H.T. Gomes, Selective biphasic oxidation of nitrogenated contaminants with H_2O_2 using polyolefin-derived carbon nanotubes, J. Environ. Chem. Eng. 13 (2025) 115128, https://doi.org/10.1016/j.jece.2024.115128.
[6] K. Voitko, A. Toth, E. Demianenko, G. Dobos, B. Berke, O. Bakalinska, A. Grebenyuk, E. Tombacz, V. Kuts, Y. Tarasenko, M. Kartel, K. Laszlo, Catalytic performance of carbon nanotubes in H_2O_2 decomposition: experimental and quantum chemical study, J. Colloid Interface Sci. 437 (2015) 283–290, https://doi.org/10.1016/j.jcis.2014.09.045.
[7] F.F. Roman, A.S. Silva, J.L. Diaz de Tuesta, A.P. Baldo, J.P.M. Lopes, G. Gonçalves, A.I. Pereira, P. Praça, A.M.T. Silva, J.L. Faria, M. Bañobre-López, H.T. Gomes, Plastic waste-derived carbon nanotubes: influence of growth catalyst and catalytic activity in CWPO, J. Environ. Chem. Eng. 13 (2025) 115206, https://doi.org/10.1016/j.jece.2024.115206.
[8] Y. Tian, Y. Li, G.-G. Ying, D. Wu, K. Shih, Y. Feng, Oxygen functionalization of carbon nanotubes shifted the formation pathway of hydroxyl radicals in catalytic ozonation: the overlooked role of hydrogen peroxide, ACS EST Eng. 4 (2024) 3021–3031, https://doi.org/10.1021/acsestengg.4c00403.
[9] J. Miao, Y. Zhu, Y. Wei, X. Wen, Z. Shao, B. Zhou, C. Wu, M. Long, Plastic wastes-derived N-doped carbon nanotubes for efficient removal of sulfamethoxazole in high salinity wastewater via nonradical peroxymonosulfate activation, J. Hazard Mater. 465 (2024) 133344, https://doi.org/10.1016/j.jhazmat.2023.133344.
[10] F.F. Roman, J.L. Diaz de Tuesta, F.K.K. Sanches, A.S. Silva, P. Marin, B.F. Machado, P. Serp, M. Pedrosa, A.M.T. Silva, J.L. Faria, H.T. Gomes, Selective denitrification of simulated oily wastewater by oxidation using Janus-structured carbon nanotubes, Catal. Today (2023) 114001, https://doi.org/10.1016/j.cattod.2023.01.008.
[11] J.L. Diaz de Tuesta, B. F. Machado, P. Serp, A.M. T. Silva, J.L. Faria, H. T. Gomes, Janus amphiphilic carbon nanotubes as Pickering interfacial catalysts for the treatment of oily wastewater by selective oxidation with hydrogen peroxide, Catal. Today 356 (2020) 205–215, https://doi.org/10.1016/j.cattod.2019.07.012.
[12] M. Enterría, J.L. Figueiredo, Nanostructured mesoporous carbons: tuning texture and surface chemistry, Carbon 108 (2016) 79–102, https://doi.org/10.1016/j.carbon.2016.06.108.
[13] R.P. Rocha, M.F.R. Pereira, J.L. Figueiredo, Metal-free carbon materials as catalysts for wet air oxidation, Catal. Today 356 (2020) 189–196, https://doi.org/10.1016/j.cattod.2019.04.047.
[14] H. Kim, E. Nam, K. An, H. Lim, Laboratory-scale plastic upcycling and green growth: evaluating the upcycling of plastic waste into carbon nanotubes from economic and environmental aspects, Chem. Eng. J. 495 (2024) 153300, https://doi.org/10.1016/j.cej.2024.153300.
[15] S.L. Wong, G.R. Mong, B.B. Nyakuma, N. Ngadi, K.Y. Wong, M.M. Hernández, S. Armenise, C.T. Chong, Upcycling of plastic waste to carbon nanomaterials: a bibliometric analysis (2000–2019), Clean. Technol. Environ. Policy 24 (2022) 739–759, https://doi.org/10.1007/s10098-021-02267-w.
[16] W.W.Y. Lau, Y. Shiran, R.M. Bailey, E. Cook, M.R. Stuchtey, J. Koskella, C.A. Velis, L. Godfrey, J. Boucher, M.B. Murphy, R.C. Thompson, E. Jankowska, A. Castillo Castillo, T.D. Pilditch, B. Dixon, L. Koerselman, E. Kosior, E. Favoino, J. Gutberlet, S. Baulch, M.E. Atreya, D. Fischer, K.K. He, M.M. Petit, U.R. Sumaila, E. Neil, M.

V. Bernhofen, K. Lawrence, J.E. Palardy, Evaluating scenarios toward zero plastic pollution, Science 369 (2020) 1455–1461, https://doi.org/10.1126/science.aba9475.
[17] K. Cao, S. Zhang, Y. Shi, X. Diao, R. Wei, N. Ji, Catalytic upgrading of plastic wastes into high-value carbon nanomaterials: synthesis and applications, ACS Nano 19 (2025) 12734–12761, https://doi.org/10.1021/acsnano.5c03391.
[18] B.N. Bhadra, Y.S. Baek, S. Kim, C.H. Choi, S.H. Jhung, Oxidative denitrogenation of liquid fuel over W2N@carbon catalyst derived from a phosphotungstinic acid encapsulated metal–azolate framework, Appl. Catal. B Environ. 285 (2021) 119842, https://doi.org/10.1016/j.apcatb.2020.119842.
[19] S. Salehian, A. Alamdari, A. Aghaeinejad-Meybodi, M.J. Azarhoosh, Highly efficient catalytic oxidative denitrogenation of fuel using CuCl-modified CNT/UiO-66, J. Environ. Chem. Eng. 13 (2025) 117182, https://doi.org/10.1016/j.jece.2025.117182.
[20] B.N. Bhadra, Y.S. Baek, C.H. Choi, S.H. Jhung, How neutral nitrogen-containing compounds are oxidized in oxidative-denitrogenation of liquid fuel with TiO(2)@carbon, Phys. Chem. Chem. Phys. 23 (2021) 8368–8374, https://doi.org/10.1039/d1cp00633a.
[21] I.R. Guimarães, A.S. Giroto, W.F. de Souza, M.C. Guerreiro, Highly reactive magnetite covered with islands of carbon: oxidation of N and S-containing compounds in a biphasic system, APPL CATAL AGEN 450 (2013) 106–113, https://doi.org/10.1016/j.apcata.2012.10.017.
[22] R.V. Mambrini, C.Z. Maia, J.D. Ardisson, P.P. de Souza, F.C.C. Moura, Fe/C and FeMo/C hybrid materials for the biphasic oxidation of fuel contaminants, N. J. Chem. 41 (2017) 142–150, https://doi.org/10.1039/c6nj02718k.
[23] A.A.S. Oliveira, A.R. Martins, R.V. Ferreira, I.T. Cunha, P. Serp, J.P. de Mesquita, F. C.C. Moura, N-doped carbon nanotubes grown on red mud residue: hybrid nanocomposites for technological applications, Catal. Today 344 (2020) 247–258, https://doi.org/10.1016/j.cattod.2019.04.060.
[24] C.V. Diniz, J.V. Nascimento, I. Binatti, P.E. Freitas, R.V. Mambrini, Hybrid catalysts based on waste electrical and electronic equipment supported on bentonite for the removal of contaminants compounds in liquid phase, Catal. Today 344 (2020) 75–83, https://doi.org/10.1016/j.cattod.2018.10.030.
[25] A.A.S. Oliveira, I.F. Teixeira, T. Christofani, J.C. Tristão, I.R. Guimarães, F.C. C. Moura, Biphasic oxidation reactions promoted by amphiphilic catalysts based on red mud residue, Appl. Catal. BEnviron. 144 (2014) 144–151, https://doi.org/10.1016/j.apcatb.2013.07.015.
[26] I.F. Teixeira, A.Ad.S. Oliveira, T. Christofani, F.C.C. Moura, Biphasic oxidation promoted by magnetic amphiphilic nanocomposites undergoing a reversible emulsion process, J. Mater. Chem. A 1 (2013) 10203–10208, https://doi.org/10.1039/c3ta11535f.
[27] J.L. Diaz de Tuesta, A. Quintanilla, D. Moreno, V.R. Ferro, J.A. Casas, Simulation and optimization of the CWPO process by combination of Aspen Plus and 6-Factor Doehlert Matrix: towards autothermal operation, Catalysts 10 (2020) 548, https://doi.org/10.3390/catal10050548.
[28] M. Zhang, Z. Xi, Z. Gong, Y. Dong, Reaction mechanism of nitrogen-containing heterocyclic compounds affecting coal spontaneous combustion, ACS Omega 8 (2023) 35295–35306, https://doi.org/10.1021/acsomega.3c05088.
[29] A.S. Silva, J.L. Diaz de Tuesta, T. Sayuri Berberich, S. Delezuk Inglez, A.R. Bertao, I. Caha, F.L. Deepak, M. Banobre-Lopez, H.T. Gomes, Doxorubicin delivery performance of superparamagnetic carbon multi-core shell nanoparticles: pH dependence, stability and kinetic insight, Nanoscale 14 (2022) 7220–7232, https://doi.org/10.1039/d1nr08550f.
[30] A.S. Silva, F.F. Roman, A.V. Dias, J.L. Diaz de Tuesta, A. Narcizo, A.P.F. da Silva, I. Çaha, F.L. Deepak, M. Bañobre-López, A.M.C. Ferrari, H.T. Gomes, Hybrid multi-core shell magnetic nanoparticles for wet peroxide oxidation of paracetamol: application in synthetic and real matrices, J. Environ. Chem. Eng. 11 (2023) 110806, https://doi.org/10.1016/j.jece.2023.110806.
[31] PlasticsEurope, Plastics - the facts 2021, 2021. Available at: ⟨https://plasticseurope.org/knowledge-hub/plastics-the-facts-2021/⟩. Accessed on: October 15th, 2025.
[32] C. Zhuo, Y.A. Levendis, Upcycling waste plastics into carbon nanomaterials: a review, J. Appl. Polym. Sci. 131 (2014) 39931, https://doi.org/10.1002/app.39931.
[33] C. Herrera, L. Barrientos, A. Rosenkranz, C. Sepulveda, J.L. García-Fierro, M. A. Laguna-Bercero, N. Escalona, Tuning amphiphilic properties of Ni/Carbon nanotubes functionalized catalysts and their effect as emulsion stabilizer for biomass-derived furfural upgrading, Fuel 276 (2020) 118032, https://doi.org/10.1016/j.fuel.2020.118032.
[34] F.F. Roman, M.C. Batista, A.S. Silva, A.J.B. Bezerra, J.L. de Diaz de Tuesta, R. V. Mambrini, A.M.T. Silva, J.L. Faria, H.T. Gomes, Polyolefin and polystyrene-derived carbon nanotubes: catalysts for oxidative desulfurization under a biphasic system, ChemCatChem 17 (2025) e202500233, https://doi.org/10.1002/cctc.202500233.
[35] A. Santos Silva, M. Seitovna Kalmakhanova, B. Kabykenovna Massalimova, J. G. Sgorlon, Dd.T. Jose Luis, H.T. Gomes, Wet peroxide oxidation of paracetamol using acid activated and Fe/Co-pillared clay catalysts prepared from natural clays, Catalysts 9 (2019) 705, https://doi.org/10.3390/catal9090705.
[36] A.L. Garcia-Costa, J.A. Zazo, J.A. Casas, UV-A assisted catalytic wet peroxide oxidation: activity of iron minerals in the degradation of DEET, Catal. Today 433 (2024) 114692, https://doi.org/10.1016/j.cattod.2024.114692.
[37] Z.A. Hussein, Z.M. Shakor, M. Alzuhairi, F. Al-Sheikh, Thermal and catalytic cracking of plastic waste: a review, Int. J. Environ. Anal. Chem. 103 (2021) 5920–5937, https://doi.org/10.1080/03067319.2021.1946527.
[38] H. Khani, O. Moradi, Influence of surface oxidation on the morphological and crystallographic structure of multi-walled carbon nanotubes via different oxidants, J. Nanostruct. Chem. 3 (2013), https://doi.org/10.1186/2193-8865-3-73.
[39] V.J. González, S.M. Vega-Díaz, A. Morelos-Gómez, K. Fujisawa, M. Endo, O. M. Cadiz, J.B. Llido, M. Terrones, H_2O_2/UV layer-by-layer oxidation of multiwall carbon nanotubes: the "onion effect" and the control of the degree of surface crystallinity and diameter, Carbon 139 (2018) 1027–1034, https://doi.org/10.1016/j.carbon.2018.07.062.
[40] Y.-L. Kuo, W.-M. Hsu, P.-C. Chiu, Y.-H. Tseng, Y. Ku, Assessment of redox behavior of nickel ferrite as oxygen carriers for chemical looping process, Ceram. Int. 39 (2013) 5459–5465, https://doi.org/10.1016/j.ceramint.2012.12.055.
[41] A.V. Ambika, N. Navya, S.R. Kiran Kumar, B.L. Suresha, Electrochemical determination of paracetamol by SWCNT-modified carbon paste electrode: a cyclic voltammetric study, Carbon Lett. 32 (2022) 1287–1295, https://doi.org/10.1007/s42823-022-00354-6.
[42] J.L. Diaz de Tuesta, A.S. Silva, F.F. Roman, L.F. Sanches, F.A. da Silva, A.I. Pereira, A.M.T. Silva, J.L. Faria, H.T. Gomes, Polyolefin-derived carbon nanotubes as magnetic catalysts for wet peroxide oxidation of paracetamol in aqueous solutions, Catal. Today 419 (2023) 114162, https://doi.org/10.1016/j.cattod.2023.114162.
[43] S. Karasawa, T. Saida, K.P. Sharma, S. Naritsuka, T. Maruyama, Single-walled carbon nanotube growth from Ni catalyst particles under conventional growth conditions by alcohol catalytic chemical vapor deposition: in situ X-ray absorption fine structure study, Jpn. J. Appl. Phys. 62 (2023) SG1036, https://doi.org/10.35848/1347-4065/acbe05.
[44] I. Nuriskasari, A.Z. Syahrial, T.A. Ivandini, A. Sumboja, B. Priyono, Q. Yan, F. Destyorini, S. Priyono, Synthesis of graphitic carbon from empty palm oil fruit bunches through single-step graphitization process using K_2FeO_4-KOH catalyst as lithium ion battery anode, Results Eng. 24 (2024) 103273, https://doi.org/10.1016/j.rineng.2024.103273.
[45] V. Tucureanu, A. Matei, A.M. Avram, FTIR spectroscopy for carbon family study, Crit. Rev. Anal. Chem. 46 (2016) 502–520, https://doi.org/10.1080/10408347.2016.1157013.
[46] A.A. Aboul-Enein, A.E. Awadallah, A.A.H. Abdel-Rahman, A.M. Haggar, Synthesis of multi-walled carbon nanotubes via pyrolysis of plastic waste using a two-stage process, Fuller. Nanotub. Carbon Nanostruct. 26 (2018) 443–450, https://doi.org/10.1080/1536383x.2018.1447929.
[47] L.M. Malard, M.A. Pimenta, G. Dresselhaus, M.S. Dresselhaus, Raman spectroscopy in graphene, Phys. Rep. 473 (2009) 51–87, https://doi.org/10.1016/j.physrep.2009.02.003.
[48] R.S. Ribeiro, A.M.T. Silva, J.L. Figueiredo, J.L. Faria, H.T. Gomes, Catalytic wet peroxide oxidation: a route towards the application of hybrid magnetic carbon nanocomposites for the degradation of organic pollutants. A review, Appl. Catal. B Environ. 187 (2016) 428–460, https://doi.org/10.1016/j.apcatb.2016.01.033.
[49] J. Rueda Márquez, I. Levchuk, M. Sillanpää, Application of catalytic wet peroxide oxidation for industrial and urban wastewater treatment: a review, Catalysts 8 (2018) 673, https://doi.org/10.3390/catal8120673.
[50] Q. Gu, Y. Ding, Z. Liu, Y. Lin, R. Schlögl, S. Heumann, D. Su, Probing the intrinsic catalytic activity of carbon nanotubes for the metal-free oxidation of aromatic thiophene compounds in ionic liquids, J. Energy Chem. 32 (2019) 131–137, https://doi.org/10.1016/j.jechem.2018.07.004.
[51] J.A. Zazo, G. Pliego, S. Blasco, J.A. Casas, J.J. Rodriguez, Intensification of the Fenton Process by Increasing the Temperature, Ind. Eng. Chem. Res. 50 (2011) 866–870, https://doi.org/10.1021/ie101963k.
[52] C. Lee, J. Yoon, Temperature dependence of hydroxyl radical formation in the hv/Fe^{3+}/H_2O_2 and Fe^{3+}/H_2O_2 systems, Chemosphere 56 (2004) 923–934, https://doi.org/10.1016/j.chemosphere.2004.04.047.
[53] A. Rey, A. Bahamonde, J.A. Casas, J.J. Rodriguez, Selectivity of hydrogen peroxide decomposition towards hydroxyl radicals in catalytic wet peroxide oxidation (CWPO) over Fe/AC catalysts, Water Sci. Technol. 61 (2010) 2769–2778, https://doi.org/10.2166/wst.2010.077.
[54] M.T. Carvajal, S. Yalkowsky, Effect of pH and ionic strength on the solubility of quinoline: back-to-basics, AAPS PharmSciTech 20 (2019) 124, https://doi.org/10.1208/s12249-019-1336-9.
[55] S.H. Standal, A.M. Blokhus, J. Haavik, A. Skauge, T. Barth, Partition coefficients and interfacial activity for polar components in oil/water model systems, J. Colloid Interface Sci. 212 (1999) 33–41, https://doi.org/10.1006/jcis.1998.5988.
[56] A. Fischbacher, C. von Sonntag, T.C. Schmidt, Hydroxyl radical yields in the Fenton process under various pH, ligand concentrations and hydrogen peroxide/Fe(II) ratios, Chemosphere 182 (2017) 738–744, https://doi.org/10.1016/j.chemosphere.2017.05.039.
[57] D. Hu, S. Liu, G. Zhang, Sonochemical treatment for removal of aqueous organic pollutants: principles, overview and prospects, Sep. Purif. Technol. 353 (2025) 128264, https://doi.org/10.1016/j.seppur.2024.128264.
[58] B.N. Bhadra, J.Y. Song, N. Uddin, N.A. Khan, S. Kim, C.H. Choi, S.H. Jhung, Oxidative denitrogenation with TiO_2@porous carbon catalyst for purification of fuel: chemical aspects, Appl. Catal. B Environ. 240 (2019) 215–224, https://doi.org/10.1016/j.apcatb.2018.09.004.
[59] I. Ahmed, S.H. Jhung, Effective aerobic oxidative denitrogenation of model fuel with metal-free porous carbon derived from phytic acid-loaded polyaniline, Chem. Eng. J. 479 (2024) 147679, https://doi.org/10.1016/j.cej.2023.147679.
[60] S. Kumari, S. Sengupta, Hierarchically porous sulfated geopolymer catalyst: preparation and performance evaluation towards oxidative denitrogenation, Catal. Lett. 154 (2023) 2932–2948, https://doi.org/10.1007/s10562-023-04519-4.
[61] M.M.H. Mondol, C.-U. Kim, S.H. Jhung, Titanium nitride@nitrogen-enriched porous carbon derived from metal–organic frameworks and melamine: a

remarkable oxidative catalyst to remove indoles from fuel, Chem. Eng. J. 450 (2022) 138411, https://doi.org/10.1016/j.cej.2022.138411.
[62] A.V. Akopyan, L.A. Kulikov, M.A. Bazhenova, N.V. Arzyaeva, A.L. Maximov, E. A. Karakhanov, Bronsted acidic catalysts based on the porous aromatic framework for effective oxidative denitrogenation, Energy Fuels 37 (2023) 13250–13259, https://doi.org/10.1021/acs.energyfuels.3c01635.
[63] S. Kumari, S. Sengupta, Kinetic modeling of dual-stage oxidative extractive denitrogenation of model fuel, Chem. Eng. Commun. 211 (2024) 1572–1587, https://doi.org/10.1080/00986445.2024.2362814.
[64] C.S. Santana, M.D. Nicodemos Ramos, C.C. Vieira Velloso, A. Aguiar, Kinetic evaluation of dye decolorization by Fenton processes in the presence of 3-hydroxyanthranilic acid, Int J. Environ. Res Public Health 16 (2019) 1602, https://doi.org/10.3390/ijerph16091602.
[65] J.L. Diaz de Tuesta, A. Quintanilla, J.A. Casas, J.J. Rodriguez, Kinetic modeling of wet peroxide oxidation with a carbon black catalyst, Appl. Catal. B Environ. 209 (2017) 701–710, https://doi.org/10.1016/j.apcatb.2017.03.031.
[66] V. Gosu, B.R. Gurjar, T.C. Zhang, R.Y. Surampalli, Oxidative degradation of quinoline using nanoscale zero-valent iron supported by granular activated carbon, J. Environ. Eng. 142 (2016), https://doi.org/10.1061/(asce)ee.1943-7870.0000981.
[67] L. Singh, P. Rekha, S. Chand, Comparative evaluation of synthesis routes of Cu/zeolite Y catalysts for catalytic wet peroxide oxidation of quinoline in fixed-bed reactor, J. Environ. Manag. 215 (2018) 1–12, https://doi.org/10.1016/j.jenvman.2018.03.021.
[68] Z. Luo, X. Li, J. Zhai, Kinetic investigations of quinoline oxidation by ferrate(VI), Environ. Technol. 37 (2016) 1249–1256, https://doi.org/10.1080/09593330.2015.1111424.
[69] N.J. Pachupate, P.D. Vaidya, Catalytic wet oxidation of quinoline over Ru/C catalyst, J. Environ. Chem. Eng. 6 (2018) 883–889, https://doi.org/10.1016/j.jece.2017.12.014.
[70] L.D.S. Pinto, L.M.F. dos Santos, R.C.D. Santos, B. Al-Duri, Supercritical water oxidation of quinoline in a continuous plug flow reactor—part 2: kinetics, J. Chem. Technol. Biotechnol. 81 (2006) 919–926, https://doi.org/10.1002/jctb.1419.
[71] Z. Li, T.J. Houser, Kinetics of the catalyzed supercritical water-quinoline reaction, Ind. Eng. Chem. Res. 31 (2002) 2456–2459, https://doi.org/10.1021/ie00011a008.
[72] W.F. Souza, M.C. Pereira, L.C. A. Oliveira, Amphiphilic catalysts based on onion-like carbon over magnetic iron oxide for petrochemical industry use, Fuel 96 (2012) 604–607, https://doi.org/10.1016/j.fuel.2012.01.011.